EVOLUTION OF FLOW CELLS WITHIN A MASS-TRANSPORT COMPLEX: INSIGHTS FROM THE GORGON SLIDE, OFFSHORE NW AUSTRALIA

HARYA D. NUGRAHA[1,2*], CHRISTOPHER A-L. JACKSON[1], HOWARD D. JOHNSON[1], and DAVID M. HODGSON[3]

[1]Basins Research Group (BRG), Imperial College, London SW7 2BP, UK

[2]Department of Geological Engineering, Universitas Pertamina, Jakarta 12220, Indonesia

[3]Stratigraphy Group, University of Leeds, Leeds LS2 9JT, UK

**email: harya.nugraha14@imperial.ac.uk*

Keywords: submarine landslide, mass-transport complex, seismic reflection, intra-flow shear, flow cells

ABSTRACT

Mass flows evolve longitudinally during emplacement, but can also vary laterally by forming discrete flow cells with different rheological states separated by shear zones. Despite being documented in many field and subsurface studies, the initiation, translation, and cessation of the flow cells remain unclear. We use five, high-quality post-stack time-migrated (PSTM) 3D seismic reflection datasets to investigate the evolution of flow cells in a seabed mass transport complex (MTC), the Gorgon Slide, on the Exmouth Plateau, offshore NW Australia. The slide originated from a 30 km-wide, NE-SW trending headwall scarp that dips steeply (*c.* 30°) seaward, and was translated to the NW over a basal-shear surface that deepens downslope (up to 500 m below seafloor). The slide is dominated by chaotic seismic facies with discrete packages of coherent reflectors, which is interpreted as a debrite that carried megaclasts (*c.* 0.05-1 km-long) derived from the headwall domain. The morphology and orientation of the basal-shear surface focused the pathway of the slide, resulting in clustering of megaclasts in proximal parts of the translation domain. The megaclasts cluster became an obstacle to flow, which resulted in the formation of two flow cells (Cells A and B) separated by a longitudinal shear zone. The interaction between the two cells is recorded by sinuous shear bands within, and ridges on

the top surface of, the slide. Along the longitudinal shear zone, the shear bands and ridges of Cell A were dragged downslope, due to Cell A impeding the movement of Cell B. This interaction suggests that Cell B travelled faster, and/or further, than Cell A, due to the absence of any flow obstacles. The abrupt cessation of Cell A is recorded by positive seabed relief, whose amplitude decreases updip. The transport processes of the Gorgon Slide show how entrainment and abrasion of megaclasts induced velocity perturbations during emplacement causing: (i) changes to the flow rheology, and (ii) initiation and cessation of flow cells. A better understanding of how flow cells evolve during MTCs transport may help to refine modelling of the potential impact of MTCs on submarine structures (e.g. pipelines, cables, etc.).

INTRODUCTION

The degradation of submarine slopes drives emplacement of large mass-transport complexes (MTCs), which are deposits of gravity-driven depositional processes that include slides, slumps and debris flows (e.g. Dott 1963; Nardin et al. 1979; Nemec 1991; Moscardelli and Wood 2008; Posamentier and Martinsen 2011). Besides their role in continental margin evolution (e.g. Gamboa et al. 2010) and petroleum system development (e.g. Weimer and Shipp 2004), MTCs also pose a significant geohazard for coastal and offshore engineering structures (e.g. Parker et al. 2008; Randolph and White 2012; Vanneste et al. 2013). Understanding the magnitude of this geohazard is essential and partly depends on the emplacement processes of the MTCs (Masson et al. 2006). For example, the rheology of MTCs can evolve during transport (Iverson 1997; Dykstra et al. 2011; Joanne et al. 2013; Ortiz-Karpf et al. 2017; Hodgson et al. 2018), which controls the amount of drag forces experienced by submarine pipelines (e.g. Zakeri 2009).

Transport processes of an MTC are dynamic, where a large, single (first-order) flow cell can evolve during its translation by (i) dilution through water ingestion (Fisher 1983; Talling et al. 2012; Sun et al. 2018); and/or (ii) formation of smaller, second-order (intra-MTC) flow cells due to internal velocity variations (Alsop and Marco 2014). In contrast to flow transformation, the formation processes of flow cells remain poorly documented. Although the nature of flow cells have been inferred from outcrop studies (Farrell 1984; Alsop and Marco 2014), limited outcrop extent invariably hampers full 3D analysis. Studies involving 3D seismic reflection data have also documented the presence of intra-MTC flow cells (Gee et al. 2005; Bull et al. 2009; Steventon et al. 2019). However, the mechanisms responsible for the initiation, translation, and cessation of these flow cells remain poorly understood. This work demonstrates that individual cells move at different speeds and/or at different times, as indicated by flow fabrics and longitudinal shears within, and on the top surface of, MTCs (*sensu* Bull et al. 2009).

Here, we study a recent MTC, the Gorgon Slide (hereafter the 'slide') that contains flow cells (Fig. 1). We use five, high-quality 3D seismic reflection datasets from the Exmouth Plateau, offshore NW Australia (Figs. 1B-C). The 3D seismic reflection datasets cover most of the Gorgon Slide area, including evacuation and deposition zones, which enable us to characterise the slide from its head to toe (Fig. 1C). As the slide is at, or just below, the seabed, detailed seismic attribute analysis allows us to: (i) document kinematic indicators on basal-shear and top surfaces, and within internal body, of the slide; (ii) reconstruct emplacement processes of the slide whose kinematic indicators serve as evidence of flow cells; (iii) infer the impact of flow cells on flow behaviour; (iv) discuss potential factors controlling the formation of the flow cells.

DATA AND METHODOLOGY

We use five, high-quality post-stack time-migrated (PSTM) 3D seismic reflection datasets that image the evacuation and most of the deposition zones of the Gorgon Slide (Figs. 1B-C). Only a small part of the slide (7%, i.e. 166 km^2 of 1760 km^2 total area) is not imaged by the 3D seismic reflection data. Thus, three 2D seismic reflection lines were used to infer the downdip limit of the deposition zone (green lines in Fig. 1C). The vertical resolution of the 3D seismic reflection data at the base of the slide (*c.* 500 mbsf) ranges from 8-11 m, based on near seabed sediment velocity and dominant frequency of 1824 m/s and 40-60 Hz, respectively. Bin spacing of the 3D seismic volumes ranges from 12.5 x 18.75 m to 20 x 25 m (see Appendix 1 for details). Depth conversion of seabed and basal-shear surface time structure maps was conducted by using average velocities of water (1519 m/s) and near seabed sediment (1824 m/s), respectively (Appendix 1). The average water velocity is constrained by ten industry wells (Fig. 1B), and the near seabed sediment velocity data is available from well ODP 762 (see Figs. 1A and 2).

The seabed and basal-shear surface of the Gorgon Slide were mapped to gain insights on the kinematics of the slide during transport. We also employed an iso-proportional slicing method (Zeng et al. 1998), midway between the seabed and basal-shear surface of the slide, to visualise heterogeneity of internal seismic facies. Several seismic attributes were used in this analysis, particularly: (i) *variance* to better image discontinuities (Chopra and Marfurt 2007), including grooves on the basal-shear surface of an MTC (e.g. Bull et al. 2009); (ii) *RMS Amplitude* to better delineate features that have distinct positive or negative amplitudes resulting from an acoustic (velocity and density) contrast (Brown 2011), such as megaclasts encased within transparent debrite (e.g. Ortiz-Karpf et al. 2017); (iii) *dip* to better image rugosity of a surface (Brown 2011), including seabed relief (e.g. Bull et al. 2009); and (iv) *spectral decomposition* of seismic reflection volume was used to highlight internal heterogeneities of a geological body (Partyka et al. 1999; Eckersley et al. 2018).

GEOLOGICAL SETTING

The Exmouth Plateau is a part of North Carnarvon Basin (NCB), a basin that experienced multiple rifting events (Fig. 2) (Tindale et al. 1998; Longley et al. 2002). Deposition during the subsequent thermal subsidence phase since the Cretaceous was initially dominated by fine-grained siliciclastic sediments, and become carbonate-dominated as the Australian plate drifted northward towards the equator (e.g. Apthorpe 1988; Hull and Griffiths 2002). Progradation of carbonate-dominated clinoforms has persisted from the Oligocene to the present-day (Fig. 2B) (Cathro et al. 2003; Moss et al. 2004). A collision between the Australian and Eurasian plates (Miocene to present-day) has reactivated optimally oriented, pre-existing rift-related faults, forming inversion structures such as the NE-SW trending Exmouth Plateau Arch (Fig. 2) (Keep et al. 1998). Emplacement of MTCs is widespread across the plateau, especially during this inversion period (Boyd et al. 1993; Hengesh et al. 2013; Scarselli et al. 2013), although pelagic carbonate sediments presently dominate the stratigraphy with sedimentation rates as low as 20 m/Ma (Golovchenko et al. 1992). We focus on the Gorgon Slide, which extends from the seabed (blue) down to its basal-shear surface (yellow, see Fig. 2B). Beneath the headwall of the Gorgon Slide, there is a rift-related horst block, which was drilled by Bluebell-1 (Fig. 2B) (McCormack and McClay 2013). This horst contains the giant Gorgon gas field, containing 11 tcf of gas in place (Clegg et al. 1992).

THE GORGON SLIDE

General Characteristics

The Gorgon Slide was evacuated from a failed slope that defines part of the present-day shelf-edge of NW Australia (Fig. 1). It was deposited in the adjacent Kangaroo Syncline, forming a lenticular, NW-SE trending feature that wedges-out to the SE (against the continental slope) and to the NW (against the eastern margin of the Exmouth Plateau Arch) (see Figs. 1B-C and 2). The slide has a maximum runout distance of *c.* 70 km. It is up to 500 m-thick and has a total volume of *c.* 500 km^3 (Fig. 3A) (Nugraha et al. 2019a). The slide terminates against two lateral margins (to the NE and SW), it is *c.* 30 km-wide in the central part and abruptly narrows to *c.* 18 km at its frontal end (Fig. 3A). These width changes form two frontal margins (eastern and western), that are separated by a NW-SE trending, *c.* 10 km-long lateral margin (Fig. 3A). The central and frontal parts of the slide display a notable along-strike change in seabed rugosity, which defines two distinctive regions: Areas A and B (Fig 3B). Area A comprises a highly rugose seabed, indicated by frequent changes of dip, and is bound by the NE lateral and eastern frontal margins (Fig. 3B). Area B comprises a relatively less rugose seabed and is bound by the SW lateral and western frontal margins (Fig. 3B). Areas A and B are separated by a linear, NW-SE trending feature (see zoomed-in image in Fig. 3B), which is subparallel to both lateral margins of the slide. This linear feature is narrow (*c.* 170-300 m-wide) and extends for *c.* 26 km, from its updip limit to the point where it merges with Area B lateral margin (see Figs. 3B-C). This feature marks the change of seabed relief between Areas A and B, where the vertical difference of relief between the two areas are variable downdip, ranging from *c.* 10 m to *c.* 20 m (Fig. 3C).

The Gorgon Slide originated from a steeply-dipping (*c.* 30°), *c.* 350 m-high headwall scarp, which forms a *c.* 18 km-long evacuation zone (Fig. 4A). The frontal margin of Area A is clearly marked by positive seabed relief (*c.* 30 m) relative to the smooth seabed bounding pre-existing strata immediately downdip. The Gorgon Slide and the pre-existing strata share similar chaotic and transparent seismic facies. Thus, the pre-existing strata are interpreted as an older MTC (Fig. 4A). A strike seismic section of the Gorgon Slide exhibits the following along-strike lateral boundaries (Fig. 4B): (i) the SW lateral margin defines the pinch-out of the slide onto substrate, and (ii) the NE lateral margin that marks the boundary with the older MTC. Sub-parallel, continuous reflections on top of the older MTC are cross-cut and overlain by overspill of the slide. Thus, these reflections are interpreted as 'paleo-seabed' (Fig. 4B). The morphology of the basal-shear surface appears to mimic that of the underlying substrate in most of Area B in the SW (Fig. 4B). In Area A, the basal-shear surface truncates underlying seismic reflections and its gradient becomes flatter adjacent to the NE lateral margin.

The linear zone on the seabed (see Figs. 3B-C) is interpreted as a longitudinal shear zone (*sensu* Bull et al. 2009), which records internal variations of transport velocity within an MTC. Occasionally, the longitudinal shear zone not only defines the change of seabed relief between Areas A and B, it could also coincide with positive seabed relief (see Fig. 4B).

The internal character of the Gorgon Slide is variable, and a seismic facies classification is used to capture this internal heterogeneity (Fig. 5). This classification captures variations in both strain and degree of internal disaggregation (i.e. flow rheology) within the MTCs (e.g. Alves et al. 2014). It builds on previous studies that have calibrated seismic reflection data with lithology from well data (e.g. Sawyer et al. 2009), as well as seismic reflections forward modelling using outcrops (Dykstra et al. 2011). Five seismic facies (SF) are defined in this study (Fig. 5A) based on variability in internal reflection configurations, both in cross-section and plan-view (see Figs. 5B-G): (i) SF-1 - mostly transparent with low-to-variable amplitude reflections, which are interpreted as debrites (cf. Posamentier and Kolla 2003; Posamentier and Martinsen 2011; Ortiz-Karpf et al. 2017); (ii) SF-2 - contains low-to-medium amplitude, discontinuous folded reflections in cross-section that occasionally forms sinuous lineations in plan-view, and also interpreted as debrites with partially disaggregated material; (iii) SF-3 - contains high-amplitude folded reflections that are offset by thrusts, interpreted as fold and thrust systems; (iv) SF-4 is characterised by isolated packages of coherent, sub-parallel reflections within a matrix composed of SF-1 and 2, interpreted as megaclasts transported within debritic matrix (cf. McGilvery 2004; Bull et al. 2009; Jackson 2011; Ortiz-Karpf et al. 2017; Hodgson et al. 2018); and (v) SF-5 is composed of sub-parallel and continuous reflections that characterise non-MTC seismic facies, i.e. progradation beneath the shelf and layered slope strata within the evacuation zone (see Fig. 4A) (e.g. Prélat et al. 2015). Internal seismic facies of the longitudinal shear zone is generally characterised by SF-1 (Fig. 3C), indicating highly disaggregated materials within the zone due to intense shearing (cf. Ogata et al. 2014; Bull and Cartwright 2019; Omeru and Cartwright 2019). However, its relatively subtle width means that the internal seismic facies are often undifferentiated from adjacent MTC bodies (Figs. 4B, and 5B-E).

To reconstruct emplacement processes, the Gorgon Slide is synthesized in terms of its kinematic indicators and internal seismic facies from four domains: (i) headwall; (ii) upper translation (UTD); (iii) lower translation (LTD); and (iv) toe (see Fig. 3B).

Headwall domain

Besides the main headwall scarp, features observed in the headwall domain (see Fig. 6) include a small scarp, circular depressions, and linear depressions updip from the main headwall scarp (see zoomed-in image in Fig. 6A). The small scarp (*c.* 10 m-high) is likely to be older than the main headwall scarp due to their cross-cutting relationship (Fig. 6B). The circular depressions have a diameter of *c.* 100 to 300 m, which are mainly distributed within the small scarp area. They are interpreted as pockmarks (e.g. Hengesh et al. 2013; Scarselli et al. 2013), which would indicate active fluid venting. The linear depressions are *c.* 3 to 5 km-long and *c.* 15 m-deep, which are interpreted as crown cracks possibly marking the location of future slope failure (Varnes 1978; Frey-Martinez et al. 2005).

In between the main headwall scarp and the evacuation-deposition zone boundary, within the evacuation zone, there are *c.* 5-16 km-long elongate features (Figs. 6A-B) with v-shaped geometries (*c.* 150-300 m-wide and *c.* 10-25 m-deep, see zoomed-in image in Fig. 6B). We interpret them as grooves (*sensu* Bull et al. 2009) that were formed due to tooling of failed materials (e.g. megaclasts) into the substrate during transport (Posamentier and Martinsen 2011; Ortiz-Karpf et al. 2017; Hodgson et al. 2018; Sobiesiak et al. 2018). Based on their orthogonal relationship with the headwall scarp, these grooves are a reliable indicator of the translation pathway of the slide through the evacuation zone.

The initial failed volume of the Gorgon Slide that was removed from the headwall domain ranges from 31 to 43 km^3, which is 12-16 times smaller than the deposited volume (*c.* 500 km^3) (Nugraha et al. 2019a). This volume discrepancy is interpreted as a result of significant erosion and substrate entrainment of the carbonate ooze substrate during transport (see Nugraha et al. 2019a).

Upper translation domain

Basal-shear surface.– Grooves observed in the updip part of the upper translation domain (Fig. 7A), are a continuation of those within the evacuation zone (see Fig. 6), displaying similar dimensions and geometries (see Headwall domain section). However, the grooves in this domain converge downslope towards the NE lateral margin (Fig. 7A), which contrasts to the more commonly described downslope-diverging grooves (e.g. Posamentier and Kolla 2003; McGilvery 2004; Ortiz-Karpf et al. 2017). This geometry implies that the pathway of the slide was focused towards the steep, NE lateral margin. As a result, the slide is thickest adjacent to this lateral margin (see Fig. 3A). The pathway was likely controlled by the morphology of the basal-shear surface that broadly follows the morphology of the underlying substrate (see Fig. 4B). This supports the observations of Ortiz-Karpf et al. (2017), who stress the impact of precursor morphology on the emplacement of MTCs.

In the central part of the basal-shear surface, there is a pair of NW-SE trending, curved lineations across the upper translation domain (Fig. 7A). They bound an area that is shallower than its surrounding area (shaded grey in Fig. 7A). These lineations appear to mark subtle changes (*c.* 10 m) in the depth of the basal-shear surface. We interpret these lineations as 'ramps' bounding an area called a 'flat' (Trincardi and Argnani 1990; Lucente and Pini 2003; Frey-Martinez et al. 2005; Bull et al. 2009). The ramps record basal erosion by the overlying slide that are commonly expressed by truncated reflections of underlying substrate by a basal-shear surface (e.g. Bull et al. 2009). However, as the ramps in this domain represent relatively small steps (i.e. 10 m), the basal-shear surface does not truncate more than one reflector.

Adjacent to the NE lateral margin, there is an area comprising highly discontinuous reflections on the variance map (Fig. 7A). Some of these discontinuous reflections form lineations oriented oblique to the NE lateral margin. This area is characterised by low-to-medium amplitude, discontinuous reflections at, and immediately beneath, the basal-shear surface (Fig. 7D). We interpret the substrate in this area to have been compressionally deformed due to stress exerted by the slide, forming a 'basal-shear zone' (Butler and McCaffrey 2010; Hodgson et al. 2018; Cardona et al. 2020).

On top of the older MTC, there is a series of lineations (0.5 to 1.5 km-long) that originate from the NE lateral margin (Figs. 7A and D). These lineations are oriented at *c.* 45° relative to the NE lateral margin. We interpret these lineations as shear fractures (i.e. Riedel shears) that developed due to strike-slip movement along the NE lateral margin. This implies that the Gorgon Slide exerted stress onto the older MTC during transport (e.g. Fleming and Johnson 1989; Martinsen 1994; Fossen 2016). Northwestwards transport of the Gorgon Slide implies that the NE lateral margin represents a dextral strike-slip fault of the Gorgon Slide relative to the older MTC (Fig. 7A). Fleming and Johnson (1989) suggest that this type of fractures is developed during an early stage of strike-slip faulting along lateral margin of the MTCs, prior to the formation of through-going lateral margins. They recorded fractures oriented at 45° clockwise from the trend of a dextral lateral margin, similar to the shear fractures found in our study.

Internal body.– The proximal part of the upper translation domain is dominated by SF-1 that surrounds scattered megaclasts (SF-4) (Fig. 7B). These megaclasts have elliptical to rectangular geometry in map-view, with long-axis lengths ranging from *c.* 0.18 to 1 km and thickness of *c.* 70 to 140 m (Fig. 7B). Seismic sections show that these megaclasts are sometimes internally folded and faulted (Fig. 7D). In the central part of this domain, the megaclasts are concentrated, forming a *c.* 15 km-long and 3 km-wide, convex-upslope cluster of megaclasts. This cluster is bound by a gradational boundary with SF-1 in the E, and an abrupt boundary in the W, which is defined by the longitudinal shear zone (Fig. 7B). Most of this cluster occurs within Area A, with a subsidiary megaclasts cluster observed within Area B, *c.* 5 km downdip (Fig. 7B). These clusters share similar frequency expressions on spectral decomposition map (Fig. 8A), and internal reflections and thicknesses (Figs. 8B-C), and are separated by the longitudinal shear zone.

Immediately downdip from the central part of the Area A megaclast cluster, partially-disaggregated materials contained within SF-2 are aligned to form a series convex-upslope bands (Fig. 7B). These bands are sub-parallel to the geometry of the cluster (Figs. 7B and 8A). In contrast, downdip from the eastern margin of the cluster, the bands show a convex-downslope geometry terminating at the NE lateral margin (Figs. 7B and 8A). A NW-SE trending, narrow area (*c.* 500 m-wide and *c.* 10 km-long) of SF-1 defines the boundary between these two sets of bands (Fig. 7B). There is a similar occurrence of convex-downslope bands downdip from the cluster in Area B (Fig. 7B). In seismic section, these bands are expressed as low-frequency, medium-amplitude folded reflections (Fig. 7D).

The scattered megaclasts in the proximal part of this domain are clustered, possibly due to downslope-convergence of the pathway of the Gorgon Slide based on the orientation of the grooves on the basal-shear surface (see Fig. 7A). The clusters of megaclasts in Areas A and B are interpreted to have been initially emplaced as a single cluster. Subsequently, they were cross-cut by the longitudinal shear zone, which was also initiated at this area (Fig. 7B).

The clusters of megaclasts were likely induced internal velocity perturbations within the slide during transport. This internal velocity variation is evidenced by the convex-downslope shear bands, in both Areas A and B, which are located downflow from the convex-upslope shear bands adjacent to the cluster of megaclasts in Area A (Fig. 7B). Another indicator of internal velocity variations is the narrow area within Area A that separates the convex-downslope and -upslope shear bands (Fig. 7B). This area is interpreted as an ‘internal shear zone’ (cf. Ogata et al. 2014; Bull and Cartwright 2019; Omeru and Cartwright 2019), containing disaggregated material due to intense shearing. Other studies have also discussed how the entrainment and abrasion of megaclasts during transport of MTCs could affect flow rheology (e.g. Joanne et al. 2013; Ortiz-Karpf et al. 2017; Hodgson et al. 2018; Sobiesiak et al. 2019), and therefore variations in intra-MTC flow velocity.

Top surface.– The top surface of the Gorgon Slide sometimes enhances the appearance of some features recorded within the internal body (Fig. 7C). For example, the internal shear bands are expressed as ridges with positive seabed relief. These ridges are terminated at the longitudinal shear zone between Areas A and B, and change their orientations (from convex-upslope to -downslope) at the internal shear zone (see Figs. 7C and 8). These ridges are interpreted as a secondary flow fabric (*sensu* Bull et al. 2009), suggesting flow velocity variation within the slide.

Lower translation domain

Basal-shear surface.– The majority of kinematic indicators observed in the upper translation domain extend to this lower translation domain (i.e. ramp, deformed substrate and shear fractures; Fig. 9A), apart from the absence of grooves. Here, the ramps are deeper (*c.* 20 m-deep, Fig. 9D), and lineations within the deformed substrate area are more apparent on the variance map (Fig. 9A). Downflow from the deformed substrate, there are SE-facing ramps (i.e. perpendicular to transport direction) that merge with the ramp that extends from the upper translation domain (Fig. 9A). Adjacent to the deformed substrate, there is a concentration of shear fractures that diminish downdip.

The ramps, deformed substrate, and shear fractures indicate that erosion and deformation also occurred in this lower translation domain (Fig. 9A). There is a close spatial relationship between the deformed substrate and the concentration of shear fractures (Fig. 9A), which also coincides with the thickest slide occurrence in Area A (Fig. 3A). This could imply that the basal and lateral substrate deformation was more severe due to increased stress exerted by the thickest part of the Gorgon Slide. However, Cardona et al. (2020), concluded from an outcrop study that there is no statistical correlation between the intensity of deformation of the basal-shear zone and the thickness of the overlying MTC.

Internal body.– The convex-upslope shear bands, between the longitudinal and internal shear zones within Area A, diminish downflow (Fig. 9B). In contrast, the convex-downslope shear bands within Area B continue and are more prominent in this lower translation domain (Fig. 9B).

Adjacent to the NE lateral margin, there is another cluster of megaclasts (Fig. 9B). In seismic section (Fig. 9D), this cluster contains megaclasts that have similar facies to those in the upper translation domain (Figs. 7D and 8B-C). However, these megaclasts have shorter long-axis (*c.* 0.05 to 0.54 km) and are thicker (*c.* 73 to 220 m) than those in the upper translation domain, i.e. *c.* 0.17 to 0.98 km-long and *c.* 70 to 137 m-thick (see Fig. 10A). Also, the megaclasts in the upper and lower translation domains show different trends of their long-axis (Fig. 10B). The megaclasts in the upper translation domain are generally trending NE-SW, and the ones in the lower translation domain are trending NNW-SSE. We also found megaclasts that are concentrated in the basal part of the slide, which are (see Fig. 9D): (i) containing chaotic and transparent internal reflections, (ii) bound by folded top, and (iii) underlain by a ramp. We name them as 'basal megaclasts'.

The presence of longitudinal and internal shear zones suggest that internal variation of flow velocity continued to occur in this domain (Fig. 9B). Between these shear zones, the gradual downflow disappearance of the convex-upslope shear bands suggests a decrease in internal velocity perturbations induced by the cluster of megaclasts in upper translation domain (see Fig. 7B).

The cluster of megaclasts adjacent to the NE lateral margin (Figs. 9B and D) are located immediately downflow from, and have similar width (2.5 km) to, the deformed substrate area (Fig. 9A). Thus, the basal and lateral substrate deformations documented on the basal-shear surface (Fig. 9A) could be related to this cluster of megaclasts, instead of reflecting the maximum thickness of the Gorgon Slide (Fig. 3A). This interpretation is supported by the same observation from the Rapanui MTD (Cardona et al. 2020), where the thickness of the deformed substrate is correlated to higher concentrations of rafted blocks (i.e. megaclasts), and not the thickness of overlying MTC. The higher concentration of megaclasts indicates an increase in flow competence overriding the area of the deformed substrate. In addition, the long-axis orientations of the megaclasts in the lower translation domain are generally oblique to sub-parallel, in contrast to the ones in the upper translation domain that are generally perpendicular, to the transport direction (Fig. 10B). Their long-axis orientations are likely to be controlled by velocity gradients (Mazzanti and De Blasio 2010), where the megaclasts in the lower translation domain are adjacent to the NE lateral margin, and experienced abrupt change of velocity gradient as they moved against the stationary older MTC (Fig. 9B). In contrast, the cluster of megaclasts in the upper translation domain experienced a lower velocity gradient, which then formed the convex-upslope geometry (Fig. 7B).

The basal megaclasts have transparent internal facies and display folded tops (Fig. 9D). We suggest they are more deformed compared to the adjacent megaclasts (Fig. 9D). Their transparent internal facies could be related to intense shearing during transport (Alves 2015; Gamboa and Alves 2015), and the folded top may be formed due to impingement of the megaclasts by the slide against the underlying ramp (see Fig. 9D) (Jackson 2011). This impingement is expressed as a positive relief of the seabed (Fig. 9D).

Top surface.– The top surface shows that the internal shear zone merges with the longitudinal shear zone in the distal part of the lower translation domain (Fig. 9C). These shear zones outline an area covering convex-upslope ridges that narrows and diminishes downflow. Consequently, Area A becomes dominated by the convex-downslope ridges (Fig. 9C). However, we can see that immediately downflow from the merging point of the shear zones, the ridges in Area A have convex-upslope geometries, most notably adjacent to the longitudinal shear zone (Fig. 9C).

The top surface supports the interpretation of kinematic indicators within the internal body of the slide (Figs. 9B-C). Here, it is also evident that velocity perturbation induced by the cluster of megaclasts in upper translation domain (Figs. 7B and 8A) had decreased, and diminished downflow, as clearly marked by the merging of the two shear zones (Fig. 9C). However, downflow from the merging point, the presence of convex-upslope ridges within Area A (terminating at the longitudinal shear zone) suggest that internal velocity perturbations continued to occur (Fig. 9C).

Toe domain

Basal-shear surface.– The basal-shear surface in this domain serves as the frontal margin of Area A, and swings through 90^o to join the lateral margin of Area B that continues downdip, beyond the 3D seismic reflection data area (Fig. 11A). The deformation style of the substrate (Fig. 11A) resembles that of the upper and lower translation domains (see Figs. 7A and 9A). In the SW part of this domain, there is a *c.* 30 m-high ramp (Figs. 10A and D), which is more profound than that in the lower translation domain (*c.* 20 m).

The geometry of the basal-shear surface indicates that Area B extends further downdip than Area A (Fig. 11A). The deformed substrate and the ramp indicate that substrate deformation and erosion continued to occur beneath the main body of the slide, despite being located the furthest from the headwall.

Internal body.– SF-1 and SF-3 (i.e. folds and thrusts system) dominate the distal part of Area A and B, respectively (Fig. 11B). The thrusts within Area B dip to the SE, sub-parallel to the transport direction of the slide (see Figs. 5G and 11B and D).

Within the older MTC (see Fig. 11B), there is a cluster of megaclasts (*c.* 2.5 km-wide and *c.* 5 km-long). The SE and SW margins of this cluster of megaclasts are defined by Area A frontal margin and Area B lateral margin, respectively (Fig. 11B). Within the cluster of megaclasts, there are lineations (NNW-SSE trending) that are broadly perpendicular to the orientation of the Area A frontal margin and the thrusts within Area B (i.e. NE-SW trending). In seismic section, these megaclasts are characterised by medium-amplitude sub-parallel reflections at the base, which become folded towards the top (Fig.

11D). The internal reflections are separated by NE-dipping thrusts. The lineations on the time-slice (Fig. 11B) correspond to these thrusts. Thus, we name this cluster of megaclasts as 'thrusted megaclasts'.

Abrupt truncation of the thrusted megaclasts by the frontal margin of Area A, and the thrusts within Area B, suggests a cross-cutting relationship (Fig. 11B). Thus, we interpret that the thrusted megaclasts had been emplaced at their present location prior to the emplacement of the Gorgon Slide. Some thrusted megaclasts (i.e. indicated by high RMS amplitude) are observed within the frontal part of Area A (Fig. 11B). However, these thrusted megaclasts are distinctly different from those of the thrust system within Area B (Fig. 11D). This suggests that the thrusted megaclasts were only entrained by the Gorgon Slide in the frontal part of the Area A (Fig. 11B). In contrast, the Area B lateral margin developed along the SW margin of the thrusted megaclasts, without any evidence of entrainment of the thrusted megaclasts by the slide within Area B.

The longitudinal shear zone that extends from the upper translation domain (see Figs. 7A and 8A) joins Area B lateral margin in the toe domain (Fig. 11B). This may indicate a relationship between the thrusted megaclasts and inferred intra-MTC velocity perturbation. Specifically, the velocity perturbation could have originated from the SW margin of the thrusted megaclasts (i.e. Area B lateral margin) and propagated upflow (Fig. 11B). Therefore, this velocity perturbation caused by the thrusted megaclasts connected with the downflow-propagating velocity perturbation induced by the cluster of megaclasts in the upper translation domain (Figs. 7B and 8A). Frey-Martínez et al. (2006) also observed similar role of pre-existing blocks (megaclasts), where a single MTC flow bifurcates to form two flows with different transport directions.

Top surface.– The rugose seabed with *c.* 30 m-high ridges relative to the flat seabed above the older MTC defines the frontal margin of Area A (see Fig. 11C). The vertical relief of the ridges of Area A is higher than in both Area B (*c.* 10 m, Fig. 11C) and the lower translation domain (*c.* 10 m, Fig. 9).

The ridges at the Area A frontal margin could indicate a buttressing effect of the slide against the thrusted megaclasts (Fig. 11C), which then formed ridges that decrease in height upflow. In contrast, the ridges in Area B are not as high as those in Area A. Thus, the slide was not buttressed against the thrusted megaclasts and it translated further downdip (Fig. 11C). These differential processes in the toe domain of Areas A and B reflect the merging between Area B lateral margin and the longitudinal shear zone (Fig. 11C).

DISCUSSION

Emplacement processes of the Gorgon Slide: a multi-cell flow emplacement mechanism

A multiple flow cell model based on field studies has been proposed by Alsop and Marco (2014), who advance the notions of Farrell (1984) of a large single-cell flow model that controls deformation patterns within an MTC. They suggest that a large (first-order) MTC consists of a number of smaller (second-order) flow cells formed during emplacement of the MTC. These smaller flow cells may interact with each other and cause overprinting on initially formed structures. Interaction between flow cells has also been documented from sonar (e.g. Prior et al. 1984; Masson et al. 1993; Gee et al. 2001) and 3D seismic reflection data (e.g. Bull et al. 2009; Steventon et al. 2019), and captured in the form of primary (longitudinal shear zone) and secondary (sinuous shear bands) flow fabrics (*sensu* Bull et al. 2009). These kinematic indicators indicate differential speeds and/or timing of downslope translating material (Masson et al. 1993; Gee et al. 2005).

In this study, the Gorgon Slide appears to comprise two intra-MTC (second-order) flow cells. These are represented physically by Areas A and B, and for the purpose of this process-based interpretation are re-named as Cells A and B, respectively. The emplacement processes of the Gorgon Slide are captured in a schematic model that recognises three stages of development (Fig. 12).

Stage 1.– Prior to slope degradation, a surface rupture might have been triggered by two main factors (Fig. 12A). First, the normal faults bounding the horst could have been inverted due to compression to destabilise the slope (Keep et al. 1998; Nugraha et al. 2019b). Second, the existence of pockmarks observed on the seabed (see Fig. 6) implies that there has been active fluid venting in the headwall area (Hengesh et al. 2013), most likely originating from the deeper gas-bearing horst block of the Gorgon Field (Fig. 2). Gas leakage into shallower sediments could have lowered the shear strength of these sediments, and primed the slope for subsequent failure (Scarselli et al. 2013). However, the Gorgon Slide was not an isolated occurrence, but rather the most recent. Previous collapse of the continental margin is reflected in the older (pre-Gorgon) MTC, which would have left a remnant topography both on the slope but especially in the area of subsequent Gorgon Slide deposition. Most notably, thrusted megaclasts had already been emplaced in the vicinity of the future toe domain of the Gorgon Slide (Fig. 12A).

Stage 2.– The arcuate geometry of the main headwall scarp indicates that the failed sediments were evacuated during a single mass-transport event (see Fig. 6). The evacuated sediments might include megaclasts derived from either the headwall and/or entrained from the layered slope substrate (Figs. 11B and 4A). During translation, the megaclasts could be deformed and fragmented (e.g. Gee et al. 2005; Alves 2015).

The downslope-converging grooves within the headwall and upper translation domains suggest a convergent pathway of the slide, resulting in the clustering of the megaclasts (Fig. 12B). In the lee-side of the cluster of megaclasts, the following features were formed: (1) convex-upslope shear bands within the slide, and (2) convex-upslope ridges on top of the slide. These features indicate slower transport velocity in and around the area of concentrated megaclasts (Fig. 12B). Higher transport velocities of flows moving around the megaclast-rich area led to the formation of the longitudinal shear zone, and the initiation of Cells A and B. The cluster of megaclasts effectively acted as an obstacle to the initial, single-cell flow. Other studies have also documented such mechanism, where the geometry of shear bands and ridges of MTCs downslope from translating megaclasts suggest slower-moving flows than surrounding materials (e.g. Masson et al. 1993; Lastras et al. 2005; Gee et al. 2006; Bull et al. 2009).

Stage 3.– The downslope propagation of the basal-shear surface was coupled with the evolution of the internal body and top surface of the slide. The area covering the convex-upslope shear bands and ridges narrowed downslope (Fig. 12C), which suggests a reduction in the influence of the cluster of megaclasts on slowing down the flow of material in its lee-side. Thus, we interpret this area as a 'shadow zone'. The shadow zone is bound by the longitudinal shear zone separating the two cells, and the internal shear zone within Cell A (Fig. 12C). The shadow zone is an example of how megaclasts influence flow processes of an MTC (e.g. Masson et al. 1993; Lucente and Pini 2003; Jackson 2011; Hodgson et al. 2018).

Downflow from the shadow zone, ridges of Cell A show convex-upslope geometries adjacent to the longitudinal shear zone. In contrast, ridges of Cell B consistently exhibit convex-downslope geometries (Fig. 12C). These geometries indicate that Cell A resisted the downslope translation of Cell B. As a result, the ridges of Cell A were dragged downslope, and the ridges of Cell B were dragged upslope (Fig. 12C). Therefore, we suggest that Cell A was travelling more slowly than Cell B. Furthermore, the high seabed relief of Cell A at the frontal margin suggest that it was forced to stop its translation by the pre-existing thrusted megaclasts (Fig. 12C), and, thus, can be considered as "stopping structures" that were formed during cessation (Masson et al. 1993; Gee et al. 2006). In contrast, the position of the thrusted megaclasts allowed Cell B to translate further downdip than Cell A. Thus, Cell B was not only travelled faster, but also further, than Cell A.

Impact of flow cells formation on MTCs flow behaviour

Submarine debris flow can travel for tens to hundreds of km across low gradient (*c.* <1^{o}) continental slope, despite its cohesive nature (Gee et al. 1999; Lastras et al. 2005). This mobility can be explained by, for instance, sustained pore-fluid pressure within the flow during transport (Major and Iverson

1999; McArdell et al. 2007), and also the presence of a thin lubricating layer of fluid at the base of the frontal part of the flow (i.e. hydroplaning, Mohrig et al. 1998). Ultimately, a debrite is formed by *en masse* freezing of the debris flow (e.g. Talling et al. 2012), where materials at flow margins (i.e. frontal and lateral) cease moving first, followed by materials in the main body of the flow (Iverson 1997).

The Gorgon Slide provides evidence of how a mass flow split into two smaller flow cells (Cell A and B, Fig. 12). The relationship between the two cells suggests that Cell A ceased movement, while Cell B was still in motion. This suggests that *en masse* freezing did not occur across the entire body of the flow synchronously. Instead, individual flow cells underwent differential timing of freezing, resulting in different runout distance of the cells. We propose that lateral friction and related pore-fluid pressure played an important role in controlling the runout distance of the two cells, in addition to the presence of pre-existing thrusted megaclasts. The longitudinal shear zone may have sustained excess pore-fluid pressure between the two cells, such that low friction between the two cells could be maintained, allowing Cell B to keep in translation despite the impediment by Cell A. In contrast, pore-fluid pressure was likely to dissipate at the lateral margins during translation (e.g. NE lateral margin, Fig. 3). The lack of excess pore-fluid pressure would have resulted in high friction between the moving slide (e.g. Cell A) and stationary lateral substrate (i.e. the older MTC). This high friction at the lateral margin was likely to reduce runout distance more significantly than the friction at the longitudinal shear zone. Such mechanisms are also observed from experimental studies (Major and Iverson 1999; De Haas et al. 2015).

Our results suggest that a debris flow comprising smaller flow cells could experience a ‘punctuated’ freezing, where a flow cell can have shorter runout distance than the others, resulting from differential friction and pore-pressure dissipation at flow cells margins. The flow behaviour documented in our study may be considered for modelling the potential impact of MTCs on subsea infrastructures.

Controls on flow cell formation

Flow cell formation within an MTC depends on internal velocity perturbations, which are controlled by variations in at least three local factors (Farrell 1984; Alsop and Marco 2011; Alsop and Marco 2014): (i) lithology and/or geometry of stratigraphic element (e.g. MTCs, channels and lobes); (ii) fluid pressures within the MTC and/or substrate; and (iii) slope and/or geometry of basal-shear surface underlying the MTC.

In the Gorgon Slide, a cluster of megaclasts within a debritic matrix initiated flow cell formation. This implies that lithology, in particular variations of the degree of disaggregation within the slide, play a key role in forming the two seismic-scale flow cells. In addition, the geometry of the basal-shear surface was also important in converging the flow, clustering the megaclasts, initiating velocity perturbation, and terminating the flow cells. Those three local variations (i.e. lithology, fluid pressures, and basal-shear surface geometry) may have been influential prior to emplacement, but their properties could also evolve during translation and cessation of the parent flow (Iverson 1997; Dykstra et al. 2011; Joanne et al. 2013; Alsop and Marco 2014; Ortiz-Karpf et al. 2017; Hodgson et al. 2018).

Origin of the pre-existing thrusted megaclasts

We have established that the thrusted megaclasts are encased by the older MTC, and, thus, had existed in their present position prior to the Gorgon Slide emplacement. Here, we discuss possible origins of the thrusted megaclasts. Deformations within, and the present location of, the thrusted megaclasts might indicate that they are either *in-situ* (remnant) or translated megaclasts.

Relatively continuous, sub-parallel reflections at the base of the thrusted megaclasts could indicate that they had not been translated (Fig. 11D). This might support the interpretation that they are *in-situ* megaclasts. However, the NE-dipping thrusts originating from the base, and folded reflections toward the top of the megaclasts, record contractional strain as a result of broadly NE-SW trending σ_1

stress (Fig. 11D). This stress was unlikely exerted by the Gorgon Slide onto the *in-situ* megaclasts, as the Gorgon Slide was transported towards the NW. Likewise, it is unlikely that the NE-dipping thrusts were formed by an older MTC that translated to the SW. This is because there is no possible source of MTCs towards the NE (see location of the NW Australian shelf, Fig. 1A).

If the thrusted megaclasts were to be deformed or translated by an MTC, the MTC should be sourced either from the Exmouth Plateau Arch (i.e. to the SW from the megaclasts) or from the NW Shelf of Australia (see Fig. 1A). As the thrusts of the megaclasts are NE-dipping (Fig. 11D), the thrusted megaclasts are unlikely to be deformed or translated by a NE-flowing MTC originated from the arch. This MTC should produce SW-dipping thrusts. Thus, the MTC forming the thrusted megaclasts was more likely sourced from the NW Shelf, similar to the source of the Gorgon Slide. However, a NW-flowing MTC should generate SE-dipping thrusts, instead of NE-dipping thrusts. This fact suggests that the thrusted megaclasts are unlikely to be deformed *in-situ*. Thus, thrusted megaclasts might be deformed during translation within the NW-flowing MTC, rotated counter-clockwise (*c.* 70-80^{o}) and then rested at their present location.

The thrusted megaclasts have similar dimensions (Figs. 13A-B) and seismic facies (Figs. 13C-D), to the basal megaclasts (see Lower translation domain section, Fig. 9D). Thus, it is possible that the thrusted megaclasts were deformed and translated by the NW-flowing MTC. Deformation and rotation of megaclasts during MTC translation have been documented in other studies, such as in Storegga Slide (Bull et al. 2009). Here, the megaclasts were re-oriented from perpendicular to become sub-parallel to transport direction with increasing distance from headwall scarp.

CONCLUSIONS

We use 3D seismic reflection data covering a recent mass-transport complex (MTC), the Gorgon Slide, from the Exmouth Plateau, offshore NW Australia, to investigate how flow cells within an MTC was formed, translated, and finally ceased. This study concludes that:

1. The Gorgon Slide was evacuated from a steep, NE-SW trending, *c.* 350 m-high headwall scarp and transported towards the NW. Layered slope strata in this headwall domain are the likely source of megaclasts that are subsequently transported downslope.
2. In the proximal part of the translation domain, downslope-converging grooves on the basal-shear surface indicate that the pathway of the slide was focused towards its lateral margin in the NE. The convergent pathway of the flow results to the clustering of the megaclasts, whose long-axes are generally trending NE-SW, perpendicular to the transport direction. This cluster of megaclasts became an obstacle to flow, causing velocity perturbation within the slide. The velocity perturbation is recoded within the internal body by convex-upslope shear bands, and on the seabed by convex-upslope ridges. These features indicate slower transport velocity of the cluster of megaclasts and materials in its lee-side. The area of the slower-moving materials narrows downslope, indicating that velocity perturbation caused by the cluster of megaclasts gradually diminished downflow, forming a 'shadow zone'. Transport velocities of flows were higher around the megaclasts, resulting in the formation of longitudinal shear zone and the initiation of two flow cells, namely Cells A and B.
3. In the distal part of the translation domain, kinematic indicators recorded on the basal-shear surface indicate that erosional and deformational processes occurred. Erosional processes are evidenced by ramp, and deformational processes are evidenced by deformed substrate or basal-shear zone and shear fractures adjacent to the NE lateral margin. The deformed substrate and shear fractures are closely related to the thickest part of the slide, comprising a cluster of megaclasts, with individual megaclasts generally trending NNW-SSE, oblique to sub-parallel to the transport direction. Shear bands within the slide and ridges on the seabed of Cell A were dragged downslope, while those of Cell B were dragged upslope. This points to Cell A acting as an impediment to the movement of faster-moving Cell B.
4. In the toe domain, the frontal margin of Cell A is marked by positive seabed relief (*c.* 30 m-high) that gradually decreases upflow, which is significantly higher than the relief of Cell B (*c.*

10 m-high). This suggests that Cell A was buttressed against a pre-existing cluster of megaclasts (i.e. encased by older MTC), while Cell B was not. Therefore, as there were no flow obstacles, Cell B was able to travel further than Cell A.

5. The morphology of the basal-shear surface and the degree of disaggregation within the slide, especially the megaclasts, played important roles in flow cell evolution. The basal-shear surface controlled the pathway of the slide, and, the clustering of the megaclasts. The megaclast clusters then induced internal velocity perturbation that could result in the initiation and cessation of intra-MTC flow cells.
6. *En masse* freezing was unlikely to occur throughout the body of the Gorgon Slide at the same time. Instead, ‘punctuated’ freezing, where Cell A has halted while Cell B was still in motion, occurred due to differential friction and pore-fluid pressure dissipation at flow cells margins. For instance, excess pore-fluid can be maintained within the longitudinal shear zone, so that Cell B only experienced minimal friction despite Cell A impeded its movement. In contrast, excess pore-fluid pressure was likely to dissipate at lateral margins (e.g. the NE lateral margin separating Cell A and stationary substrate). Thus, Cell A experienced higher lateral friction than that of Cell B, resulting in reduced runout distance. This punctuated freezing mechanism may be considered for modelling the impact of MTCs on submarine infrastructures.

ACKNOWLEDGEMENT

We thank Geoscience Australia for providing seismic and borehole data. Schlumberger and Geoteric are thanked for providing software licenses to Imperial College London. The first author thanks the Indonesia Endowment Fund for Education (LPDP) (Grant No.: 20160822019161) for its financial support.

CONFLICT OF INTEREST

No conflict of interest declared.

REFERENCES

Alsop, G.I., and Marco, S., 2011, Soft-sediment deformation within seismogenic slumps of the Dead Sea Basin: Journal of Structural Geology, v. 33, p. 433-457.

Alsop, G.I., and Marco, S., 2014, Fold and fabric relationships in temporally and spatially evolving slump systems: A multi-cell flow model: Journal of Structural Geology, v. 63, p. 27-49.

Alves, T.M., Kurtev, K., Moore, G.F., and Strasser, M., 2014, Assessing the internal character, reservoir potential, and seal competence of mass-transport deposits using seismic texture: A geophysical and petrophysical approach: AAPG Bulletin, v. 98, p. 793-824.

Alves, T.M., 2015, Submarine slide blocks and associated soft-sediment deformation in deep-water basins: A review: Marine and Petroleum Geology, v. 67, p. 262-285.

Apthorpe, M., 1988, Cainozoic depositional history of the North West Shelf: The North West Shelf, Australia: Petroleum Exploration Society of Australia, p. 55-84.

Boyd, R., Williamson, P., and Haq, B., 1993, Seismic Stratigraphy and Passive-Margin Evolution of the Southern Exmouth Plateau, *in* Posamentier, H.W., Summerhayes, C.P., Haq, B.U., and Allen, G.P., eds., Sequence Stratigraphy and Facies Associations: Oxford, Blackwell Scientific Publications, p. 579-603.

Brown, A.R., 2011, Interpretation of three-dimensional seismic data: AAPG Memoir 42, SEG Investigations in Geophysics No. 9: Tulsa, The American Association of Petroleum Geologists and the Society of Exploration Geophysicists.

Bull, S., Cartwright, J., and Huuse, M., 2009, A review of kinematic indicators from mass-transport complexes using 3D seismic data: Marine and Petroleum Geology, v. 26, p. 1132-1151.

Bull, S., and Cartwright, J.A., 2019, Line length balancing to evaluate multi-phase submarine landslide development: an example from the Storegga Slide, Norway: Geological Society, London, Special Publications, v. 500.

Butler, R., and McCaffrey, W., 2010, Structural evolution and sediment entrainment in mass-transport complexes: outcrop studies from Italy: Journal of the Geological Society, v. 167, p. 617-631.

Cardona, S., Wood, L.J., Dugan, B., Jobe, Z., and Strachan, L.J., 2020, Characterization of the Rapanui mass-transport deposit and the basal shear zone: Mount Messenger Formation, Taranaki Basin, New Zealand: Sedimentology.

Cathro, D.L., Austin Jr, J.A., and Moss, G.D., 2003, Progradation along a deeply submerged OligoceneMiocene heterozoan carbonate shelf: How sensitive are clinoforms to sea level variations?: AAPG bulletin, v. 87, p. 1547-1574.

Chopra, S., and Marfurt, K.J., 2007, Seismic attributes for prospect identification and reservoir characterization, v. 11, Society of Exploration Geophysicists Tulsa, Oklahoma.

Clegg, L., Sayers, M., and Tait, A., 1992, The Gorgon Gas Field: Chapter 32.

De Haas, T., Braat, L., Leuven, J.R., Lokhorst, I.R., and Kleinhans, M.G., 2015, Effects of debris flow composition on runout, depositional mechanisms, and deposit morphology in laboratory experiments: Journal of Geophysical Research: Earth Surface, v. 120, p. 1949-1972.

Dott, R., 1963, Dynamics of subaqueous gravity depositional processes: AAPG Bulletin, v. 47, p. 104-128.

Dykstra, M., Garyfalou, K., Kertznus, V., Kneller, B., Milana, J.P., Molinaro, M., Szuman, M., and Thompson, P., 2011, Mass-transport deposits: Combining outcrop studies and seismic forward modeling to understand lithofacies distributions, deformations, and their seismic stratigraphic expression: SEPM Special Publication, v. 96, p. 293-310.

Eckersley, A.J., Lowell, J., and Szafian, P., 2018, High-definition frequency decomposition: Geophysical Prospecting, v. 66, p. 1138-1143.

Farrell, S.G., 1984, A dislocation model applied to slump structures, Ainsa Basin, South Central Pyrenees: Journal of Structural Geology, v. 6, p. 727-736.

Fisher, R.V., 1983, Flow transformations in sediment gravity flows: Geology, v. 11, p. 273-274.

Fleming, R.W., and Johnson, A.M., 1989, Structures associated with strike-slip faults that bound landslide elements: Engineering Geology, v. 27, p. 39-114.

Fossen, H., 2016, Structural geology, Cambridge University Press.

Frey-Martinez, J., Cartwright, J., and Hall, B., 2005, 3D seismic interpretation of slump complexes: examples from the continental margin of Israel: Basin Research, v. 17, p. 83-108.

Frey-Martínez, J., Cartwright, J., and James, D., 2006, Frontally confined versus frontally emergent submarine landslides: A 3D seismic characterisation: Marine and Petroleum Geology, v. 23, p. 585-604.

Gamboa, D., Alves, T., Cartwright, J., and Terrinha, P., 2010, MTD distribution on a 'passive' continental margin: The Espírito Santo Basin (SE Brazil) during the Palaeogene: Marine and Petroleum Geology, v. 27, p. 1311-1324.

Gamboa, D., and Alves, T.M., 2015, Three-dimensional fault meshes and multi-layer shear in mass-transport blocks: Implications for fluid flow on continental margins: Tectonophysics, v. 647, p. 21-32.

Gee, M., Masson, D., Watts, A., and Allen, P., 1999, The Saharan debris flow: an insight into the mechanics of long runout submarine debris flows: Sedimentology, v. 46, p. 317-335.

Gee, M., Gawthorpe, R., and Friedmann, J., 2005, Giant striations at the base of a submarine landslide: Marine Geology, v. 214, p. 287-294.

Gee, M., Gawthorpe, R., and Friedmann, S., 2006, Triggering and evolution of a giant submarine landslide, offshore Angola, revealed by 3D seismic stratigraphy and geomorphology: Journal of Sedimentary Research, v. 76, p. 9-19.

Gee, M.J., Masson, D.G., Watts, A.B., and Mitchell, N.C., 2001, Passage of debris flows and turbidity currents through a topographic constriction: seafloor erosion and deflection of flow pathways: Sedimentology, v. 48, p. 1389-1409.

Golovchenko, X., Borella, P.E., and O'Connell, S.B., 1992, Sedimentary cycles on the Exmouth Plateau, *in* Von Rad, U., Haq, B.U., Kidd, R.B., and O'Connell, S.B., eds., Proceedings of the Ocean Drilling Program, Scientific Results: College Station, TX, Ocean Drilling Program, p. 279-291.

Hengesh, J.V., Dirstein, J.K., and Stanley, A.J., 2013, Landslide geomorphology along the Exmouth Plateau continental margin, North West Shelf, Australia: Australian Geomechanics, v. 48, p. 71-92.

Hodgson, D., Brooks, H., Ortiz-Karpf, A., Spychala, Y., Lee, D., and Jackson, C.-L., 2018, Entrainment and abrasion of megaclasts during submarine landsliding and their impact on flow behaviour: Geological Society, London, Special Publications, v. 477, p. SP477. 26.

Hull, J.N.F., and Griffiths, C.M., 2002, Sequence stratigraphic evolution of the Albian to Recent section of the Dampier Sub-basin, NorthWest Shelf, Australia: The Sedimentary Basins of Western Australia 3: Proceedings of the Petroleum Exploration Society of Australia Symposium, p. 617-639.

Iverson, R.M., 1997, The physics of debris flows: Reviews of geophysics, v. 35, p. 245-296.

Jackson, C.A., 2011, Three-dimensional seismic analysis of megaclast deformation within a mass transport deposit; implications for debris flow kinematics: Geology, v. 39, p. 203-206.

Joanne, C., Lamarche, G., and Collot, J.Y., 2013, Dynamics of giant mass transport in deep submarine environments: the Matakaoa Debris Flow, New Zealand: Basin Research, v. 25, p. 471-488.

Keep, M., Powell, C., and Baillie, P., 1998, Neogene deformation of the North West Shelf, Australia: The sedimentary basins of Western Australia, v. 2, p. 81-91.

Lastras, G., De Blasio, F.V., Canals, M., and Elverhøi, A., 2005, Conceptual and numerical modeling of the BIG'95 debris flow, western Mediterranean Sea: Journal of Sedimentary Research, v. 75, p. 784-797.

Longley, I.M., Buessenschuett, C., Clydsdale, L., Cubitt, C.J., Davis, R.C., Johnson, M.K., Marshall, N.M., Murray, A.P., Somerville, R., and Spry, T.B., 2002, The North West Shelf of Australia - a Woodside Perspective, *in* Keep, M., and Moss, S.J., eds., The Sedimentary Basins of Western Australia 3: Petroleum Exploration Society of Australia Symposium: Perth, p. 28-88.

Lucente, C.C., and Pini, G.A., 2003, Anatomy and emplacement mechanism of a large submarine slide within a Miocene foredeep in the northern Apennines, Italy: A field perspective: American Journal of Science, v. 303, p. 565-602.

Major, J.J., and Iverson, R.M., 1999, Debris-flow deposition: Effects of pore-fluid pressure and friction concentrated at flow margins: Geological Society of America Bulletin, v. 111, p. 1424-1434.

Martinsen, O., 1994, Mass movements, The geological deformation of sediments, Springer, p. 127-165.

Masson, D., Huggett, Q., and Brunsden, D., 1993, The surface texture of the Saharan debris flow deposit and some speculations on submarine debris flow processes: Sedimentology, v. 40, p. 583-598.

Masson, D., Harbitz, C., Wynn, R., Pedersen, G., and Løvholt, F., 2006, Submarine landslides: processes, triggers and hazard prediction: Philosophical Transactions of the Royal Society A: Mathematical, Physical and Engineering Sciences, v. 364, p. 2009-2039.

Mazzanti, P., and De Blasio, F., 2010, Peculiar morphologies of subaqueous landslide deposits and their relationship to flow dynamics, Submarine mass movements and their consequences, Springer, p. 141-151.

McArdell, B.W., Bartelt, P., and Kowalski, J., 2007, Field observations of basal forces and fluid pore pressure in a debris flow: Geophysical research letters, v. 34.

McCormack, K., and McClay, K., 2013, Structural Architecture of the Gorgon Platform, North West Shelf, Australia: The Sedimentary Basins of Western Australia IV: Proceedings of the Petroleum Exploration Society of Australia Symposium, Perth, WA, p. 24.

McGilvery, T.A.H., Geoffrey, 2004, Seafloor and shallow subsurface examples of mass transport complexes, Offshore Brunei, Offshore Technology Conference: Houston.

Mohrig, D., Ellis, C., Parker, G., Whipple, K.X., and Hondzo, M., 1998, Hydroplaning of subaqueous debris flows: Geological Society of America Bulletin, v. 110, p. 387-394.

MOSCARDELLI, L., AND WOOD, L., 2008, New classification system for mass transport complexes in offshore Trinidad: Basin Research, v. 20, p. 73-98.

MOSS, G.D., CATHRO, D.L., AND AUSTIN, J.A., 2004, Sequence biostratigraphy of prograding clinoforms, northern Carnarvon Basin, Western Australia: a proxy for variations in Oligocene to Pliocene global sea level?: Palaios, v. 19, p. 206-226.

NARDIN, T.R., HEIN, F., GORSLINE, D.S., AND EDWARDS, B., 1979, A review of mass movement processes sediment and acoustic characteristics, and contrasts in slope and base-of-slope systems versus canyon-fan-basin floor systems.

NEMEC, W., 1991, Aspects of sediment movement on steep delta slopes, *in* Colella, A., and Prior, D.B., eds., Coarsed-Grained Deltas, International Association of Sedimentologists, p. 29-73.

NUGRAHA, H.D., JACKSON, C.A.-L., JOHNSON, H.D., HODGSON, D.M., AND CLARE, M., 2019a, How erosive are submarine landslides?, EarthArXiv.

NUGRAHA, H.D., JACKSON, C.A., JOHNSON, H.D., HODGSON, D.M., AND REEVE, M.T., 2019b, Tectonic and oceanographic process interactions archived in Late Cretaceous to Present deep-marine stratigraphy on the Exmouth Plateau, offshore NW Australia: Basin Research, v. 31, p. 405-430.

OGATA, K., MOUNTJOY, J., PINI, G.A., FESTA, A., AND TINTERRI, R., 2014, Shear zone liquefaction in mass transport deposit emplacement: a multi-scale integration of seismic reflection and outcrop data: Marine Geology, v. 356, p. 50-64.

OMERU, T., AND CARTWRIGHT, J.A., 2019, The efficacy of kinematic indicators in a complexly deformed Mass Transport Deposit: Insights from the deepwater Taranaki Basin, New Zealand: Marine and Petroleum Geology, v. 106, p. 74-87.

ORTIZ-KARPF, A., HODGSON, D.M., JACKSON, C.A.-L., AND MCCAFFREY, W.D., 2017, Influence of Seabed Morphology and Substrate Composition On Mass-Transport Flow Processes and Pathways: Insights From the Magdalena Fan, Offshore Colombia: Journal of Sedimentary Research, v. 87, p. 189-209.

PARKER, E.J., TRAVERSO, C.M., MOORE, R., EVANS, T., AND USHER, N., 2008, Evaluation of landslide impact on deepwater submarine pipelines: Offshore technology conference.

PARTYKA, G., GRIDLEY, J., AND LOPEZ, J., 1999, Interpretational applications of spectral decomposition in reservoir characterization: The Leading Edge, v. 18, p. 353-360.

POSAMENTIER, H.W., AND KOLLA, V., 2003, Seismic geomorphology and stratigraphy of depositional elements in deep-water settings: Journal of Sedimentary Research, v. 73, p. 367-388.

POSAMENTIER, H.W., AND MARTINSEN, O.J., 2011, The character and genesis of submarine mass-transport deposits: insights from outcrop and 3D seismic data: Mass-transport deposits in deepwater settings: Society for Sedimentary Geology (SEPM) Special Publication 96, p. 7-38.

PRÉLAT, A., PANKHANIA, S.S., JACKSON, C.A.-L., AND HODGSON, D.M., 2015, Slope gradient and lithology as controls on the initiation of submarine slope gullies; Insights from the North Carnarvon Basin, Offshore NW Australia: Sedimentary Geology, v. 329, p. 12-17.

PRIOR, D.B., BORNHOLD, B., AND JOHNS, M., 1984, Depositional characteristics of a submarine debris flow: The Journal of Geology, v. 92, p. 707-727.

RANDOLPH, M.F., AND WHITE, D.J., 2012, Interaction forces between pipelines and submarine slides—A geotechnical viewpoint: Ocean Engineering, v. 48, p. 32-37.

SAWYER, D.E., FLEMINGS, P.B., DUGAN, B., AND GERMAINE, J.T., 2009, Retrogressive failures recorded in mass transport deposits in the Ursa Basin, Northern Gulf of Mexico: Journal of Geophysical Research: Solid Earth, v. 114.

SCARSELLI, N., MCCLAY, K., AND ELDERS, C., 2013, Submarine slide and slump complexes, Exmouth Plateau, NW Shelf of Australia: The Sedimentary Basins of Western Australia IV: Proceedings of the Petroleum Exploration Society of Australia Symposium.

SOBIESIAK, M.S., KNELLER, B., ALSOP, G.I., AND MILANA, J.P., 2018, Styles of basal interaction beneath mass transport deposits: Marine and Petroleum Geology, v. 98, p. 629-639.

SOBIESIAK, M.S., BUSO, V.V., KNELLER, B., ALSOP, G.I., AND MILANA, J.P., 2019, Block Generation, Deformation, and Interaction of Mass-Transport Deposits With the Seafloor: An Outcrop-

Based Study of the Carboniferous Paganzo Basin (Cerro Bola, NW Argentina): Submarine Landslides: Subaqueous Mass Transport Deposits from Outcrops to Seismic Profiles, p. 91-104.

Steventon, M.J., Jackson, C.A., Hodgson, D.M., and Johnson, H.D., 2019, Strain analysis of a seismically imaged mass-transport complex, offshore Uruguay: Basin Research, v. 31, p. 600-620.

Sun, Q., Alves, T., Lu, X., Chen, C., and Xie, X., 2018, True volumes of slope failure estimated from a Quartenary mass-transport deposit in the northern South China Sea: Geophysical Research Letters.

Talling, P.J., Masson, D.G., Sumner, E.J., and Malgesini, G., 2012, Subaqueous sediment density flows: Depositional processes and deposit types: Sedimentology, v. 59, p. 1937-2003.

Tindale, K., Newell, N., Keall, J., and Smith, N., 1998, Structural evolution and charge history of the Exmouth Sub-basin, Northern Carnarvon Basin, Western Australia, *in* Purcell, P.G., and Purcell, R.R., eds., The Sedimentary Basins of Western Australia 2: Proceedings of the Petroleum Exploration Society of Australia: Perth, p. 473-490.

Trincardi, F., and Argnani, A., 1990, Gela submarine slide: a major basin-wide event in the Plio-Quaternary foredeep of Sicily: Geo-Marine Letters, v. 10, p. 13.

Vanneste, M., Forsberg, C.F., Glimsdal, S., Harbitz, C.B., Issler, D., Kvalstad, T.J., Løvholt, F., and Nadim, F., 2013, Submarine landslides and their consequences: what do we know, what can we do?, Landslide science and practice, Springer, p. 5-17.

Varnes, D.J., 1978, Slope movement types and processes: Special report, v. 176, p. 11-33.

Weimer, P., and Shipp, C., 2004, Mass Transport Complexes: Musing on past uses and suggestions for future directions, Offshore Technology Conference: Houston.

Zakeri, A., 2009, Review of state-of-the-art: Drag forces on submarine pipelines and piles caused by landslide or debris flow impact: Journal of offshore mechanics and Arctic engineering, v. 131.

Zeng, H., Henry, S.C., and Riola, J.P., 1998, Stratal slicing, Part II: Real 3-D seismic data: Geophysics, v. 63, p. 514-522.

FIGURE CAPTIONS

Fig. 1.--- A) Location of the study area. Regional seismic line (orange) across several wells (see Fig. 2). **B)** Seabed map of the Gorgon Slide, and industry well data (red dots) available for this study. The Gorgon Slide is expressed as rugose relief on the seabed. Both evacuation and most of deposition zones are imaged within the 3D seismic reflection data. **C)** Outline of the deposits of the Gorgon Slide (dark grey), where a minor area (c. 7%) of the total slide area in the NW (dashed line) is not imaged within the 3D seismic reflection data. This minor part is delineated using 2D seismic lines (green). Five 3D seismic reflection datasets (Gorgon, Acme, Draeck, Duyfken, and Io-Jansz) were used in this study. Bathymetry and topography data are from Geoscience Australia.

Fig. 2.--- A regional seismic section across the Exmouth Plateau (see Fig. 1 for location). **A)** Uninterpreted. **B)** Interpreted. The Gorgon Slide is bound by a basal-shear surface (yellow) at the base and seabed (blue) at the top. Modified from Nugraha et al. (2019b).

Fig. 3.--- A) Thickness map of the Gorgon Slide showing lateral boundaries of the slide (i.e. NE lateral margin and pinch-out in the SW), with thickness concentration adjacent to the NE lateral margin. We divide rugged geometry of the frontal margin into eastern and western frontal margins. **B)** Seabed dip map showing two distinct sub-bodies (namely Area A and B) within the slide. The two areas are separated by a zone of longitudinal shear. The depositional zone of the slide comprises upper (UTD) and lower (LTD) translation and toe domains. **C)** A 3D perspective of seabed structure map in the LTD showing the geometry of the longitudinal shear zone.

Fig. 4.--- A) Dip-oriented seismic section across the Gorgon Slide showing the headwall scarp, evacuation and deposition zones. **B)** Strike-oriented seismic section showing the asymmetric geometry of the slide, with erosional lateral margin in the NE and pinch-out in the SW.

Fig. 5.--- Seismic facies classification used in this study. **A)** Seismic facies description and interpretation. **B)** Variance attributes extraction between the basal-shear surface and an iso-

proportional surface (50% between the basal-shear surface and the seabed). **C-E)** Seismic sections showing seismic facies within the translation domain. **F)** A time-slice of variance attribute extraction (see G for position) showing seismic facies in the toe domain. **G)** A seismic section showing seismic facies in the toe domain.

Fig. 6.--- Seabed map showing kinematic indicators in the headwall domain, which include the main headwall of the Gorgon Slide, grooves, crown cracks, pockmarks, and a small scarp. **A)** Uninterpreted. **B)** Interpreted.

Fig. 7.--- Upper translation domain of the Gorgon Slide. **A)** Basal-shear surface variance map (top) and its interpretation (bottom). **B)** Internal body RMS amplitude map (extracted 50 ms above and below isoproportional horizon, orange) (top) and its interpretation (bottom). **C)** Top surface dip map (top) and its interpretation (bottom). **D)** Seismic sections, uninterpreted (above) and interpreted (bottom), showing seismic facies across the upper translation domain. See text for discussions.

Fig. 8.--- A) Spectral decomposition map within the slide (50% between basal-shear and top surfaces) showing features within upper translation domain in detail. **B)** Uninterpreted, and **C)** interpreted, seismic section along megaclasts (SF-4) across Area A and B. See text for discussion.

Fig. 9.--- Lower translation domain of the Gorgon Slide. **A)** Basal-shear surface variance map (top) and its interpretation (bottom). **B)** Internal body RMS amplitude map (extracted 50 ms above and below isoproportional horizon, orange) (top) and its interpretation (bottom). **C)** Top surface dip map (top) and its interpretation (bottom). **D)** Seismic sections, uninterpreted (above) and interpreted (bottom), showing seismic facies across the upper translation domain. See text for discussion.

Fig. 10.--- Dimensions and orientation of the megaclasts in the upper and translation domains. **A)** Megaclasts in the upper translation domain are generally thinner with longer long-axes, as compared to the ones in the lower translation domain that are thicker with shorter long-axes. **B)** Megaclasts in

the upper translation domain are generally oriented perpendicular, and the ones in the lower translation domain are oblique to sub-parallel, to the transport direction.

Fig. 11.--- Toe domain of the Gorgon Slide. **A)** Basal-shear surface variance map (top) and its interpretation (bottom). **B)** Internal body RMS amplitude map (time-slice at the orange horizon in D) (top) and its interpretation (bottom). **C)** Top surface dip map (top) and its interpretation (bottom). **D)** Seismic sections, uninterpreted (above) and interpreted (bottom), showing seismic facies across the toe domain. See text for discussion.

Fig. 12.--- Schematic diagram of Gorgon Slide depicting three stages of emplacement processes. **A)** A failure event occurred. **B)** The slide split into two flow cells, Cell A and B, due to a cluster of megaclasts derived from the headwall and/or slope strata that acted as a flow obstacle. **C)** Cell A ceased, and its frontal margin is expressed on the seabed, while Cell B flowed beyond the limit of the dataset. See text for discussion.

Fig. 13.--- A) Variance map extracted along the orange horizon in C-D, overlaid by time structure map of thrusted megaclasts (see the red horizon in D, left). The thrusted megaclasts define the frontal margin of Cell A and lateral margin of Cell B. **B)** Variance map extracted along the basal-shear surface (yellow) in C-D, overlaid by time structure map of the basal megaclasts (see the red horizon in D, right). **C)** Uninterpreted, and **D)** interpreted seismic section across the thrusted and basal megaclasts. These megaclasts have similar dimension and seismic facies, thus, likely to have a similar origin.

Figure 1

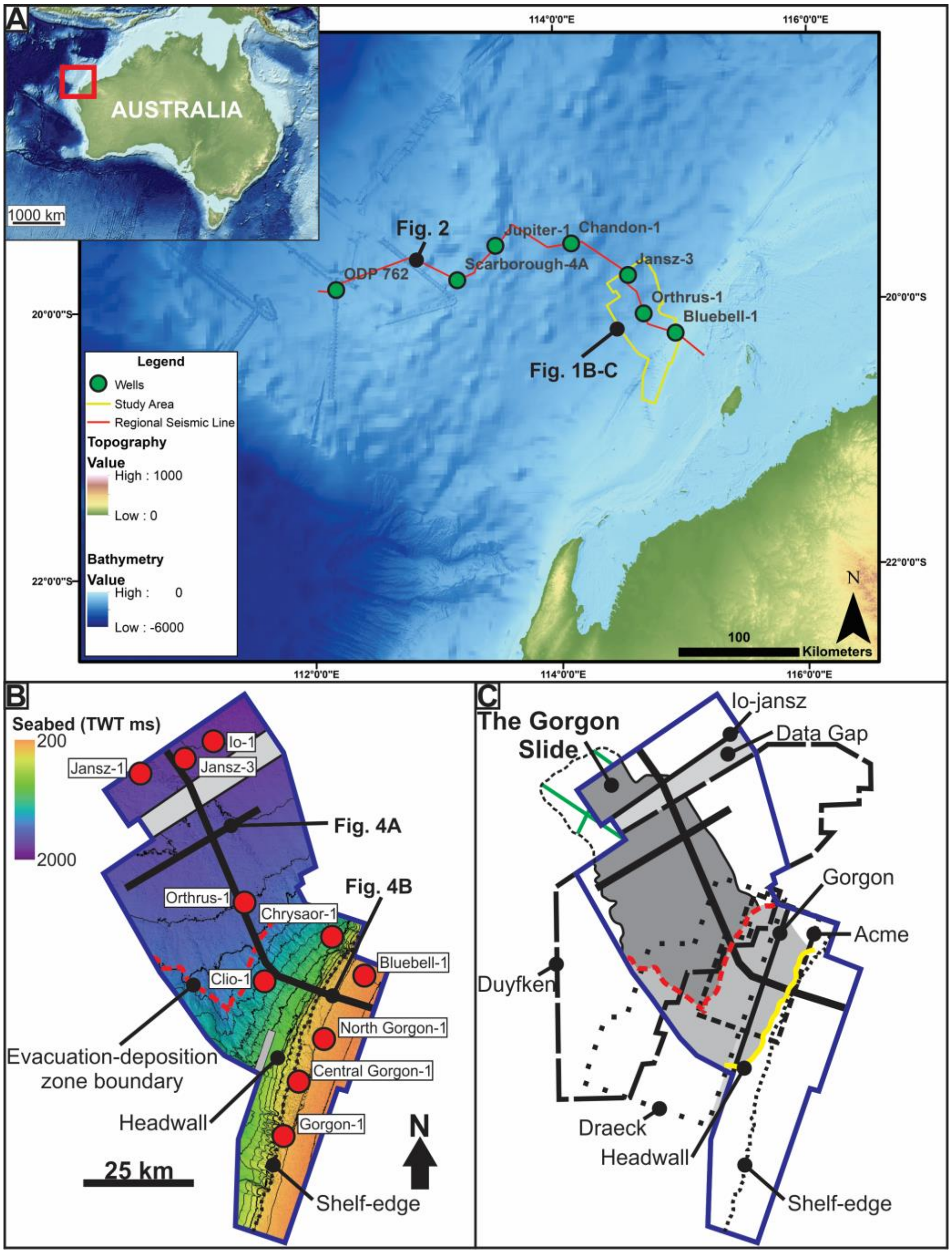

A
AUSTRALIA
1000 km
114°0'0"E
116°0'0"E
112°0'0"E
20°0'0"S
22°0'0"S
Fig. 2
ODP 762
Scarborough-4A
Jupiter-1
Chandon-1
Jansz-3
Orthrus-1
Bluebell-1
Fig. 1B-C
Legend
Wells
Study Area
Regional Seismic Line
Topography
Value
High : 1000
Low : 0
Bathymetry
Value
High : 0
Low : -6000
N
100
Kilometers
B
Seabed (TWT ms)
200
2000
Io-1
Jansz-1
Jansz-3
Fig. 4A
Fig. 4B
Orthrus-1
Chrysaor-1
Bluebell-1
Clio-1
North Gorgon-1
Central Gorgon-1
Gorgon-1
Evacuation-deposition zone boundary
Headwall
Shelf-edge
25 km
N
C
The Gorgon Slide
Io-jansz
Data Gap
Gorgon
Acme
Duyfken
Draeck
Headwall
Shelf-edge

840 Figure 2

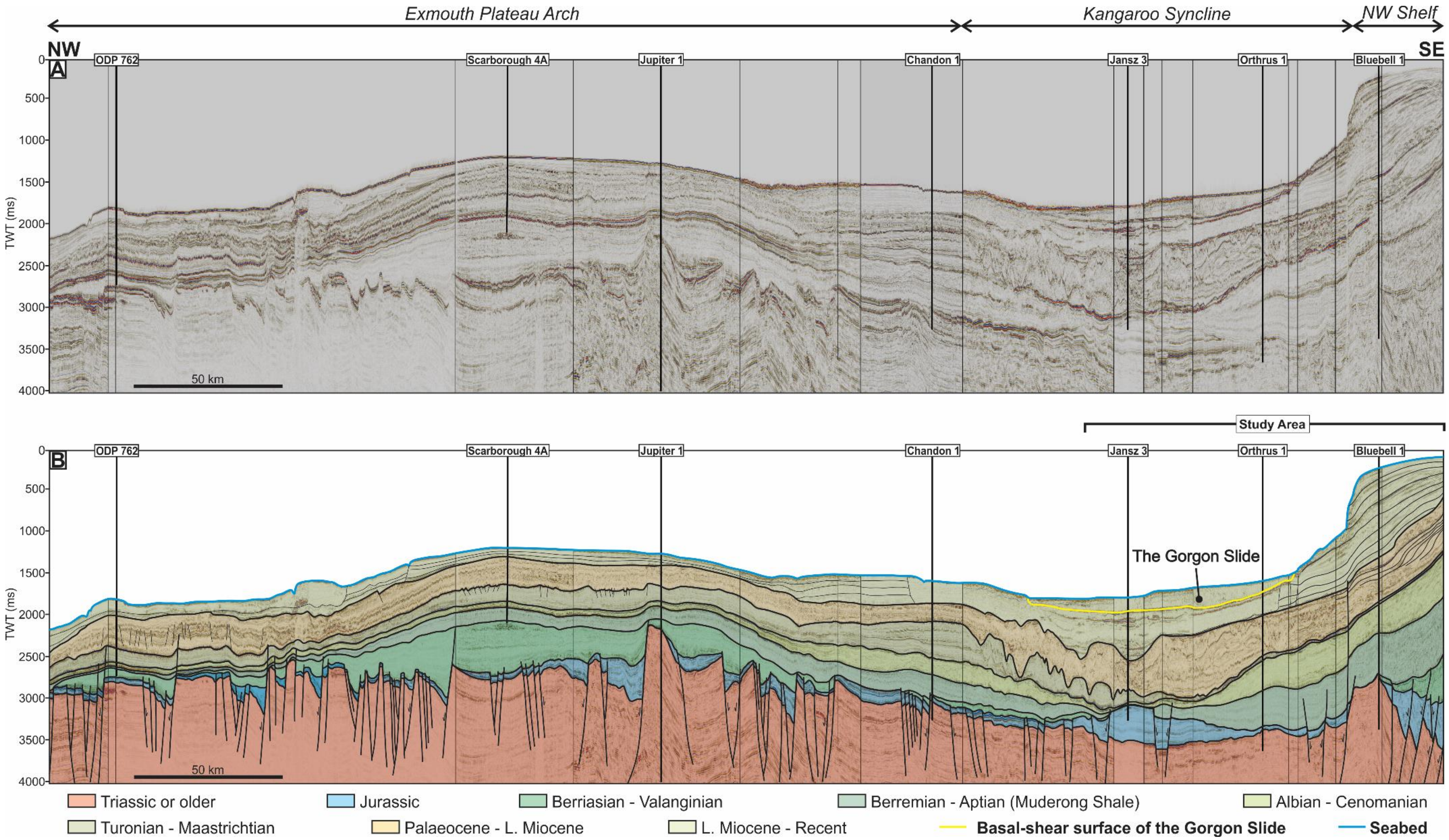

841

842 Figure 3

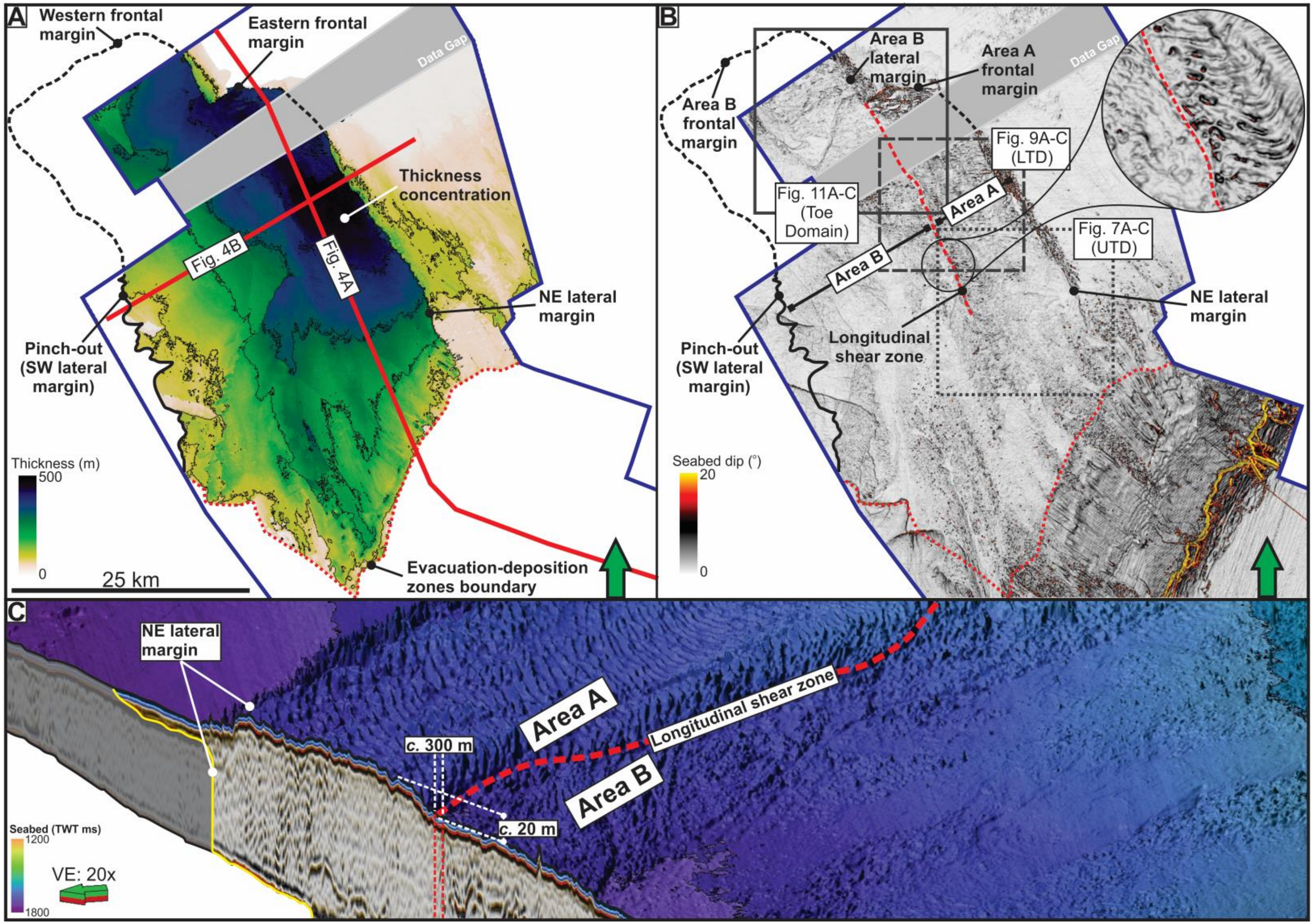

843

844 Figure 4

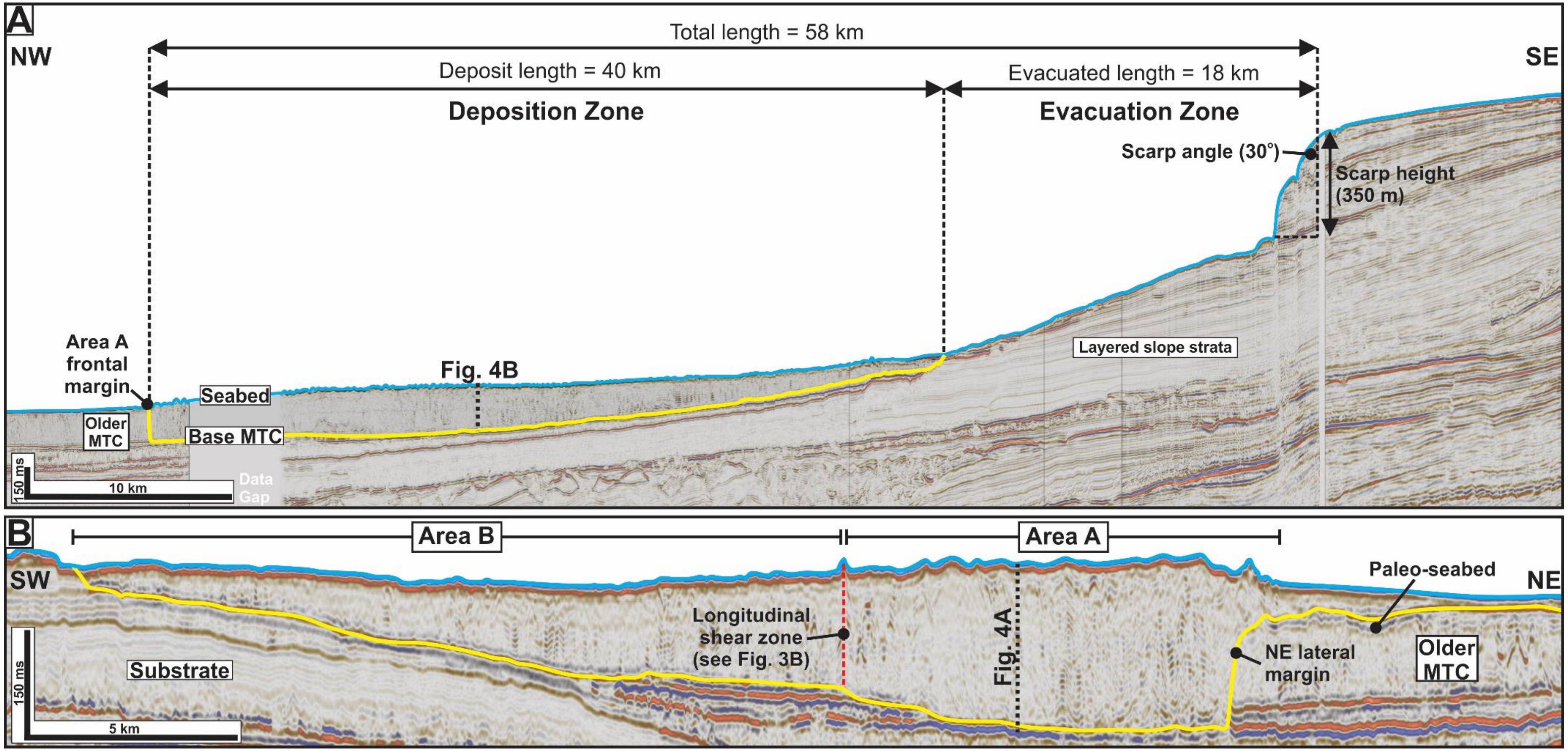

845

Figure 5

A Facies	Description	Interpretation
SF-1	Chaotic and transparent both in cross-section and map-view (Fig. 5B-C).	Debrites containing disaggregated materials (cf. Posamentier and Kolla 2003).
SF-2	Low-to-medium amplitude, discontinuous folded reflections that occasionally form sinuous lineations in map-view (Fig. 5B, D-E).	Debrites containing partially disaggregated materials (cf. Ortiz-Karpf et al. 2017).
SF-3	High amplitude, discontinuous folded reflections that are separated by imbricate thrusts (Fig. 5F-G).	Fold and thrust systems formed by compressional deformation within MTCs, flow direction is generally perpendicular to the strike of the thrusts (Bull et al. 2009).
SF-4	Isolated packages of coherent, sub-parallel reflections within a matrix composed of SF-1 or 2 (Fig. 5B-C, E). In most cases, the reflections are disrupted, e.g. faulted and folded.	Megaclasts transported within debritic matrix (cf. Bull et al. 2009; Jackson 2011; Hodgson et al. 2018).
SF-5	Medium-to-high amplitude, continuous, sub-parallel, downslope-dipping reflections beneath the shelf and within the evacuation zone (Fig. 4A).	Non-MTC deposits, i.e. carbonate progradation and layered slope deposits that were the source of, and eroded by, the Gorgon Slide (Hengesh et al. 2013; Nugraha et al. 2019b).

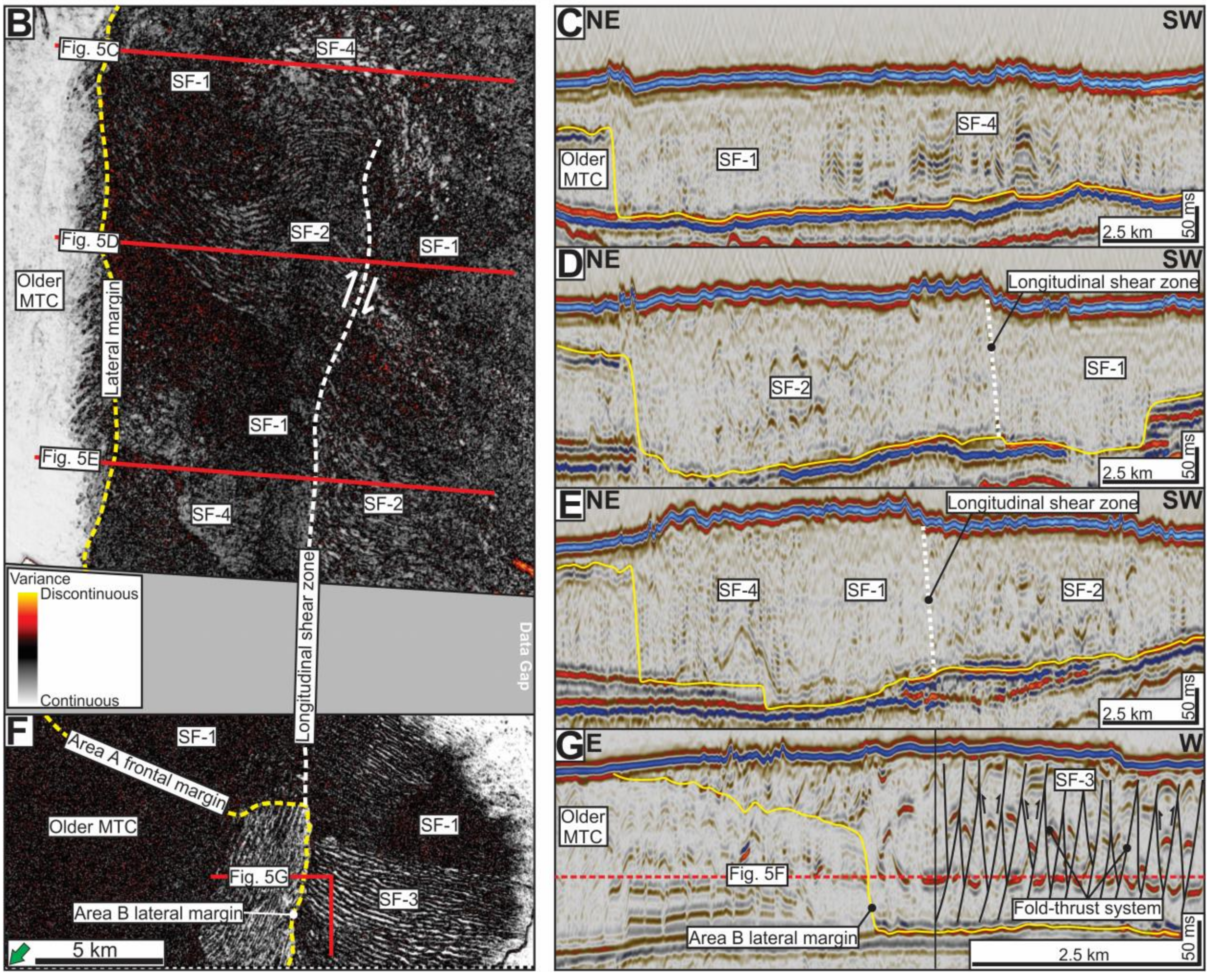

848 Figure 6

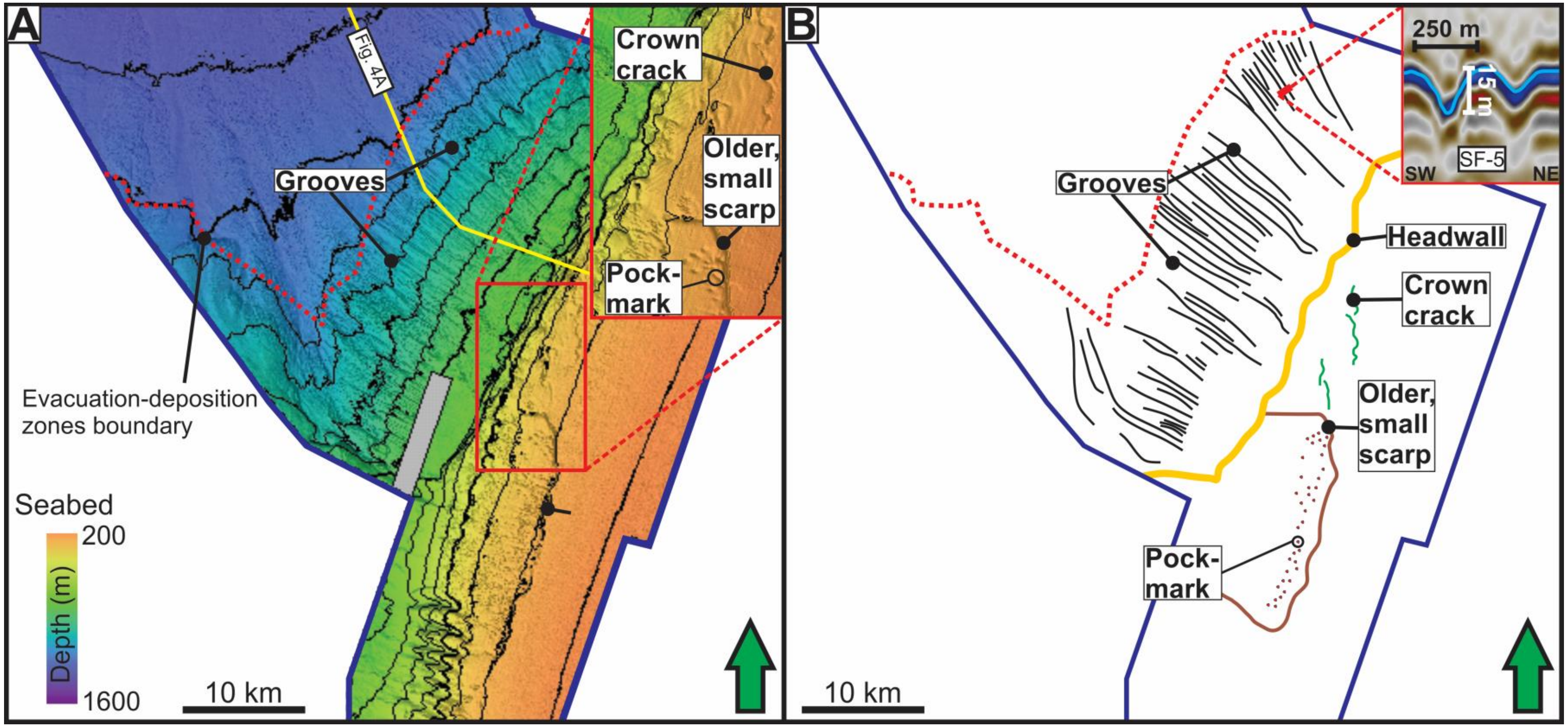

849

Figure 7

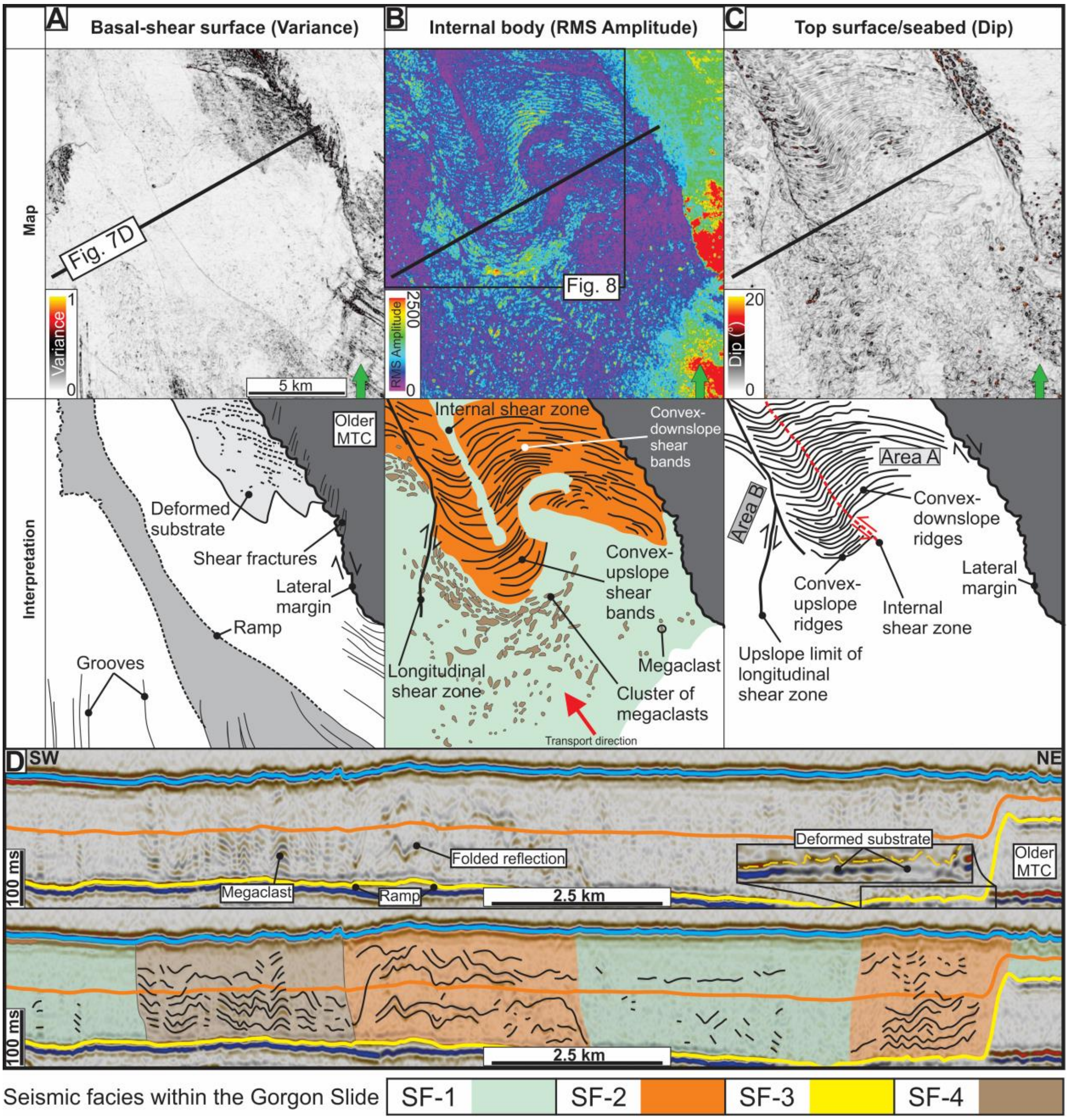

A
Basal-shear surface (Variance)
B
Internal body (RMS Amplitude)
C
Top surface/seabed (Dip)
Map
Interpretation
Fig. 7D
Variance
1
0
5 km
Fig. 8
RMS Amplitude
2500
0
Dip (°)
20
0
Older MTC
Deformed substrate
Shear fractures
Lateral margin
Ramp
Grooves
Internal shear zone
Convex-downslope shear bands
Convex-upslope shear bands
Megaclast
Longitudinal shear zone
Cluster of megaclasts
Transport direction
Area A
Area B
Convex-downslope ridges
Lateral margin
Convex-upslope ridges
Internal shear zone
Upslope limit of longitudinal shear zone
D
SW
NE
100 ms
Megaclast
Ramp
Folded reflection
2.5 km
Deformed substrate
Older MTC
100 ms
2.5 km
Seismic facies within the Gorgon Slide
SF-1
SF-2
SF-3
SF-4

Figure 8

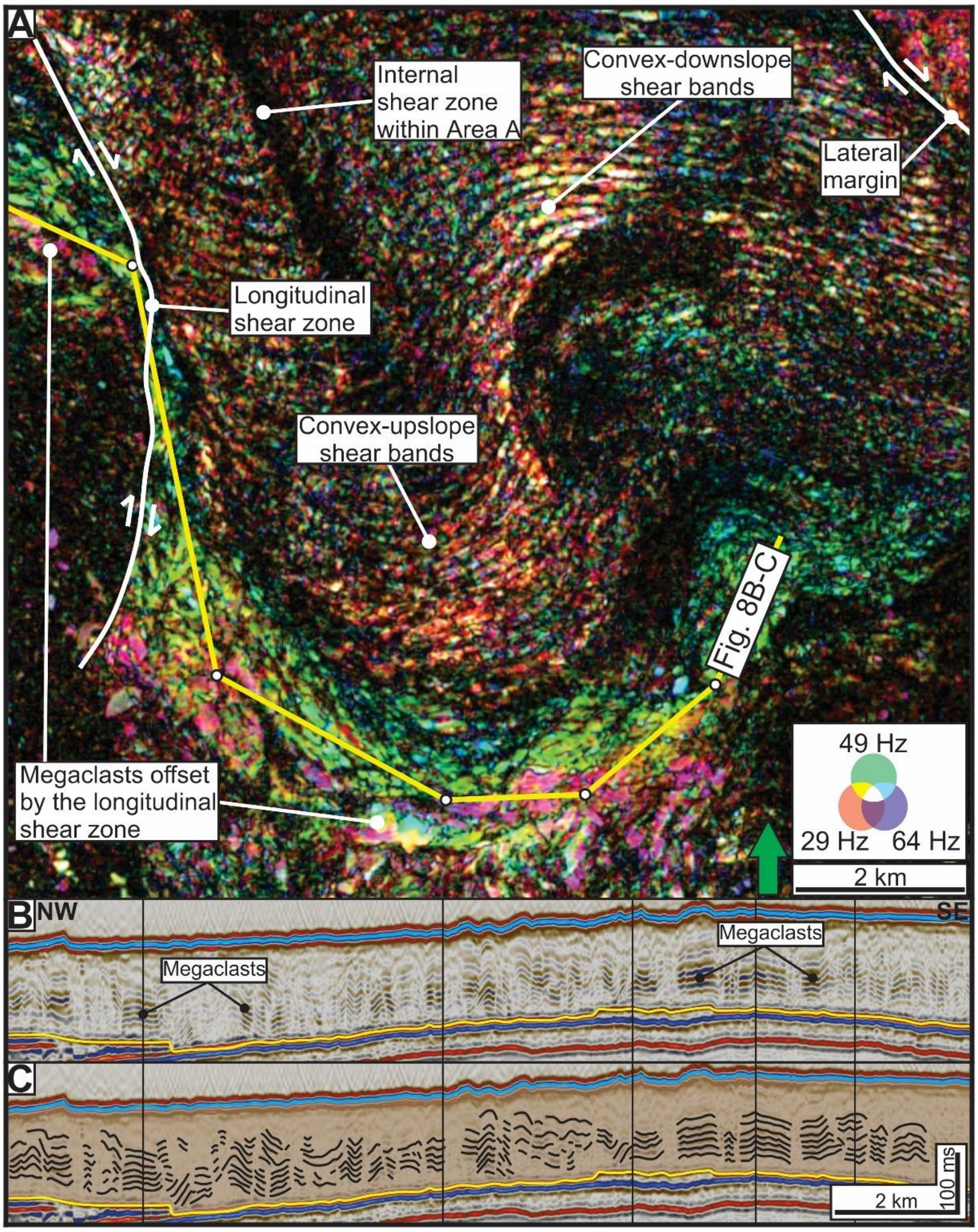
A
Internal shear zone within Area A
Convex-downslope shear bands
Lateral margin
Longitudinal shear zone
Convex-upslope shear bands
Fig. 8B-C
Megaclasts offset by the longitudinal shear zone
49 Hz
29 Hz
64 Hz
2 km
B
NW
SE
Megaclasts
Megaclasts
C
2 km
100 ms

Figure 9

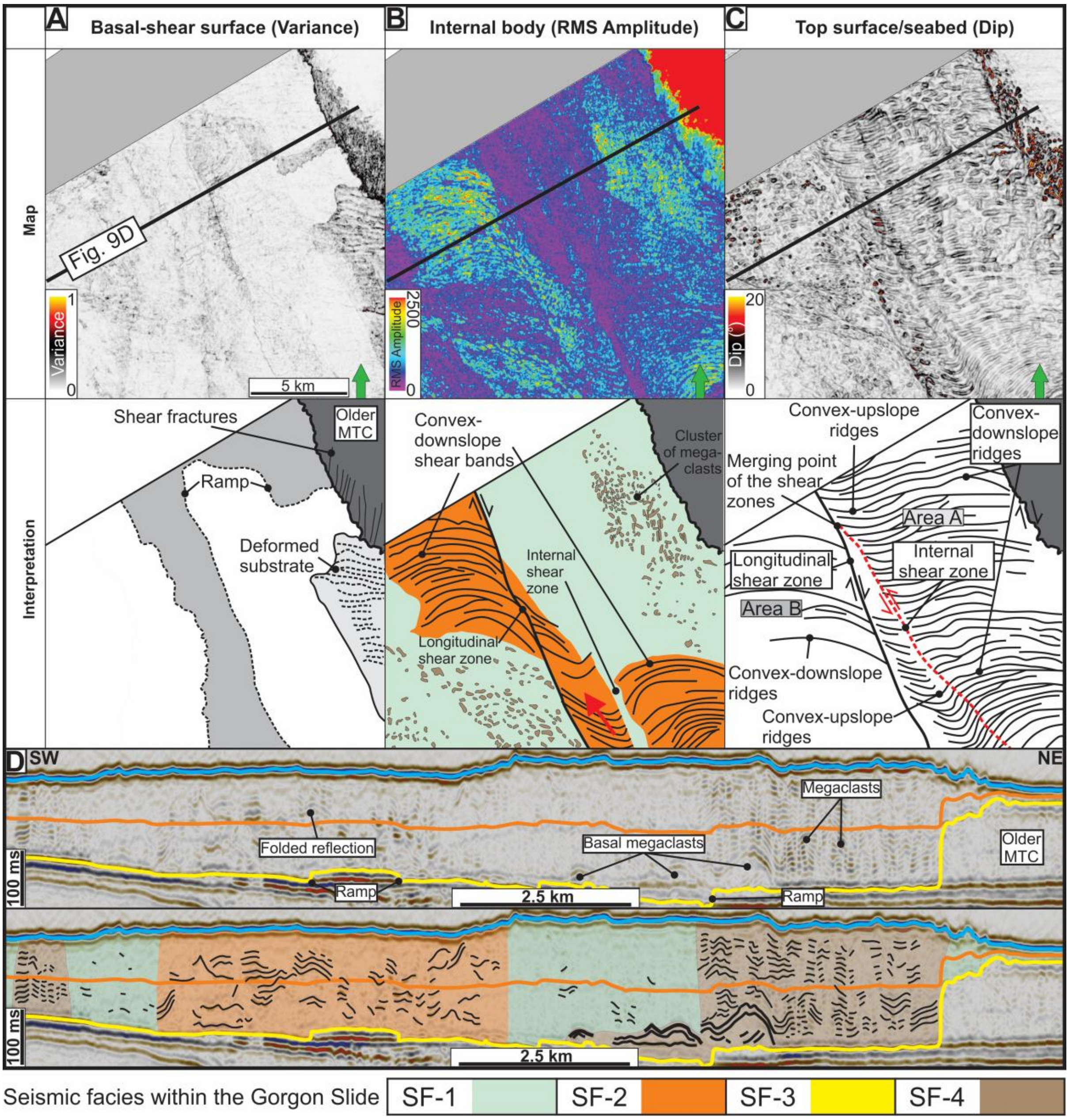
A
Basal-shear surface (Variance)
B
Internal body (RMS Amplitude)
C
Top surface/seabed (Dip)
Map
Interpretation
Fig. 9D
Variance
1
0
5 km
RMS Amplitude
2500
0
Dip (°)
20
0
Shear fractures
Older MTC
Ramp
Deformed substrate
Convex-downslope shear bands
Cluster of mega-clasts
Internal shear zone
Longitudinal shear zone
Convex-upslope ridges
Convex-downslope ridges
Merging point of the shear zones
Area A
Longitudinal shear zone
Internal shear zone
Area B
Convex-downslope ridges
Convex-upslope ridges
D
SW
NE
Megaclasts
Folded reflection
Basal megaclasts
Older MTC
100 ms
Ramp
2.5 km
Ramp
100 ms
2.5 km
Seismic facies within the Gorgon Slide
SF-1
SF-2
SF-3
SF-4

Figure 10

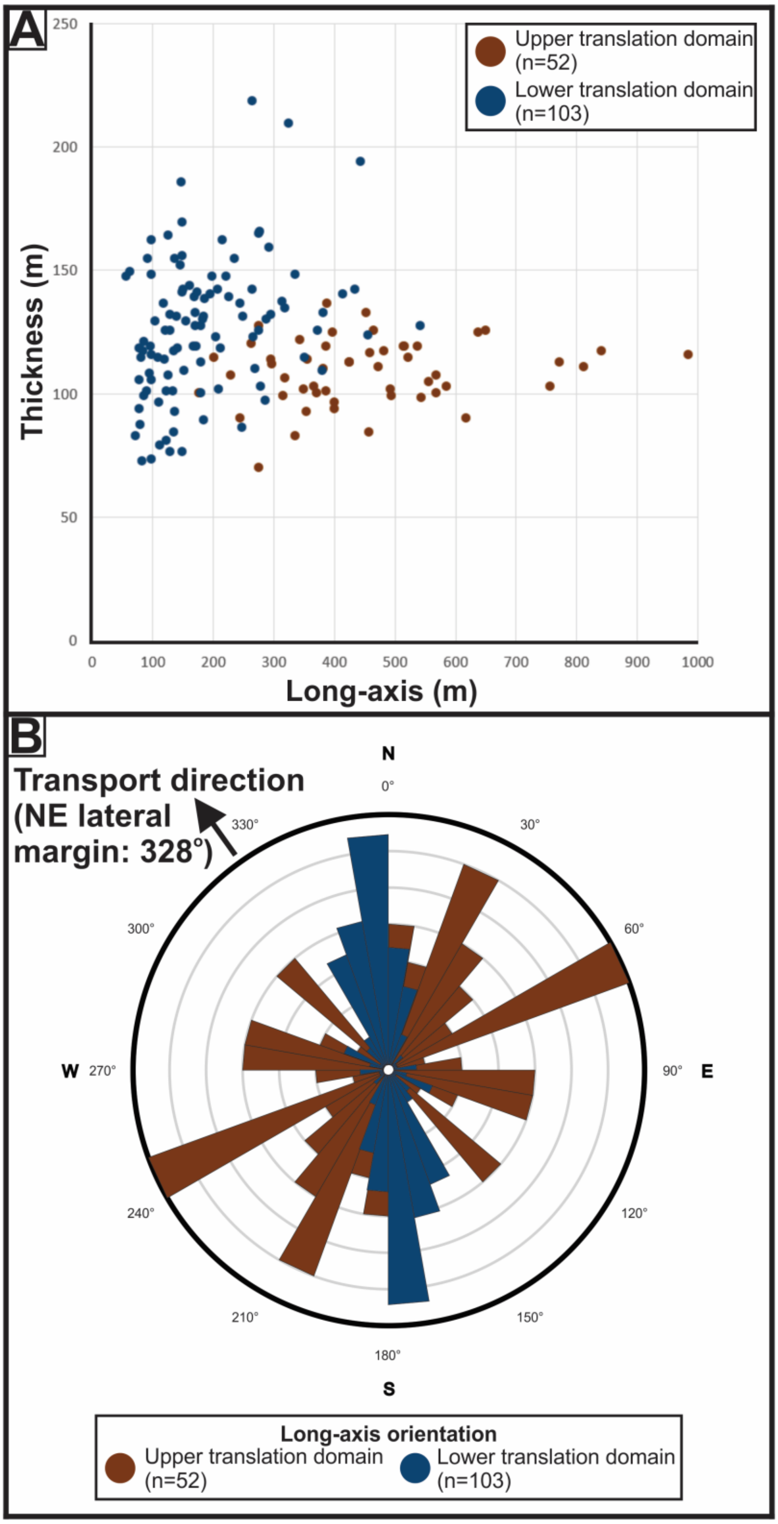
A
Upper translation domain (n=52)
Lower translation domain (n=103)
Thickness (m)
Long-axis (m)
0
50
100
150
200
250
0
100
200
300
400
500
600
700
800
900
1000
B
Transport direction (NE lateral margin: 328°)
N
0°
30°
60°
90°
E
120°
150°
180°
S
210°
240°
W
270°
300°
330°
Long-axis orientation
Upper translation domain (n=52)
Lower translation domain (n=103)

858 Figure 11

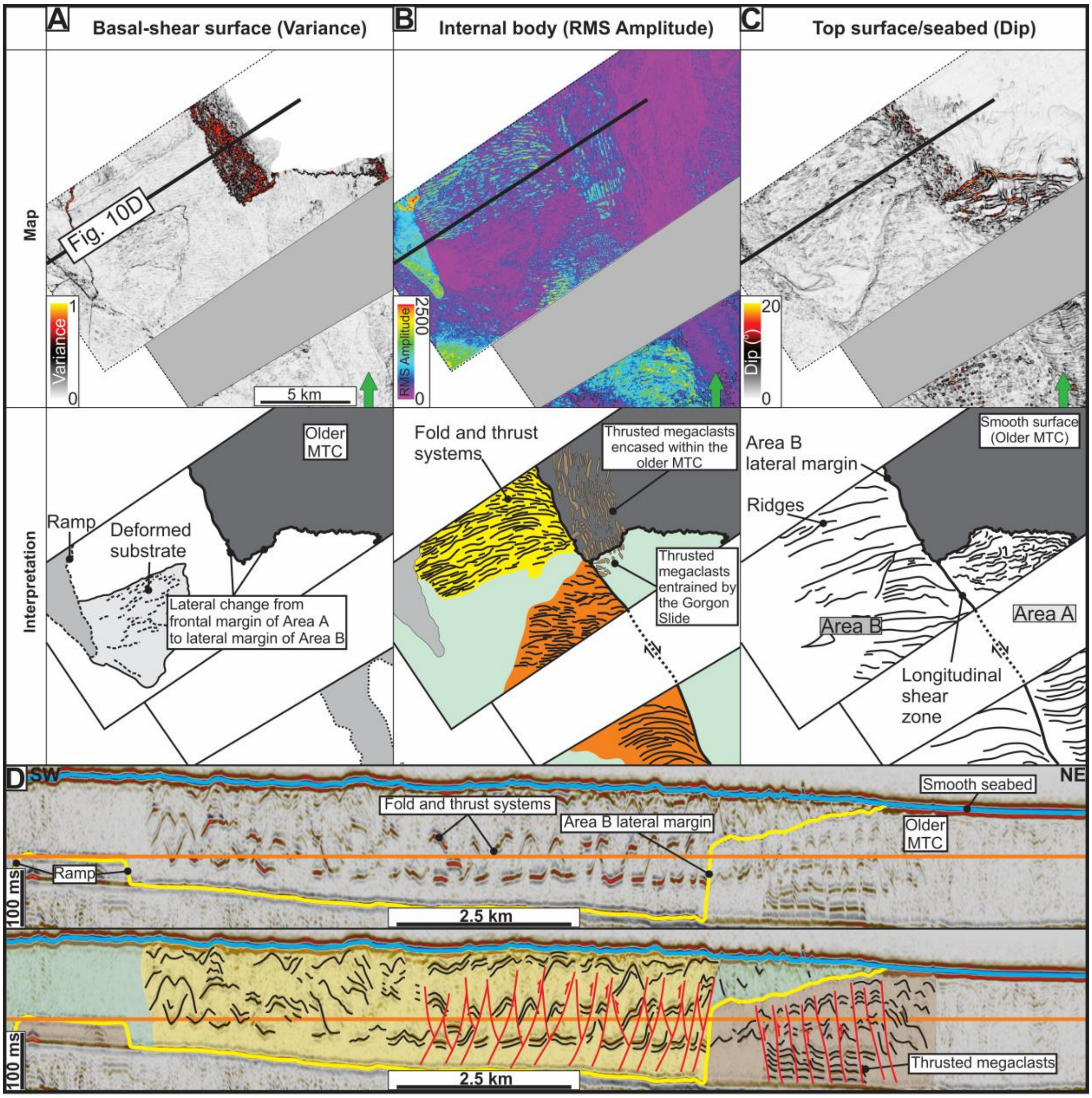

859 Seismic facies within the Gorgon Slide | SF-1 | SF-2 | SF-3 | SF-4

860 Figure 12

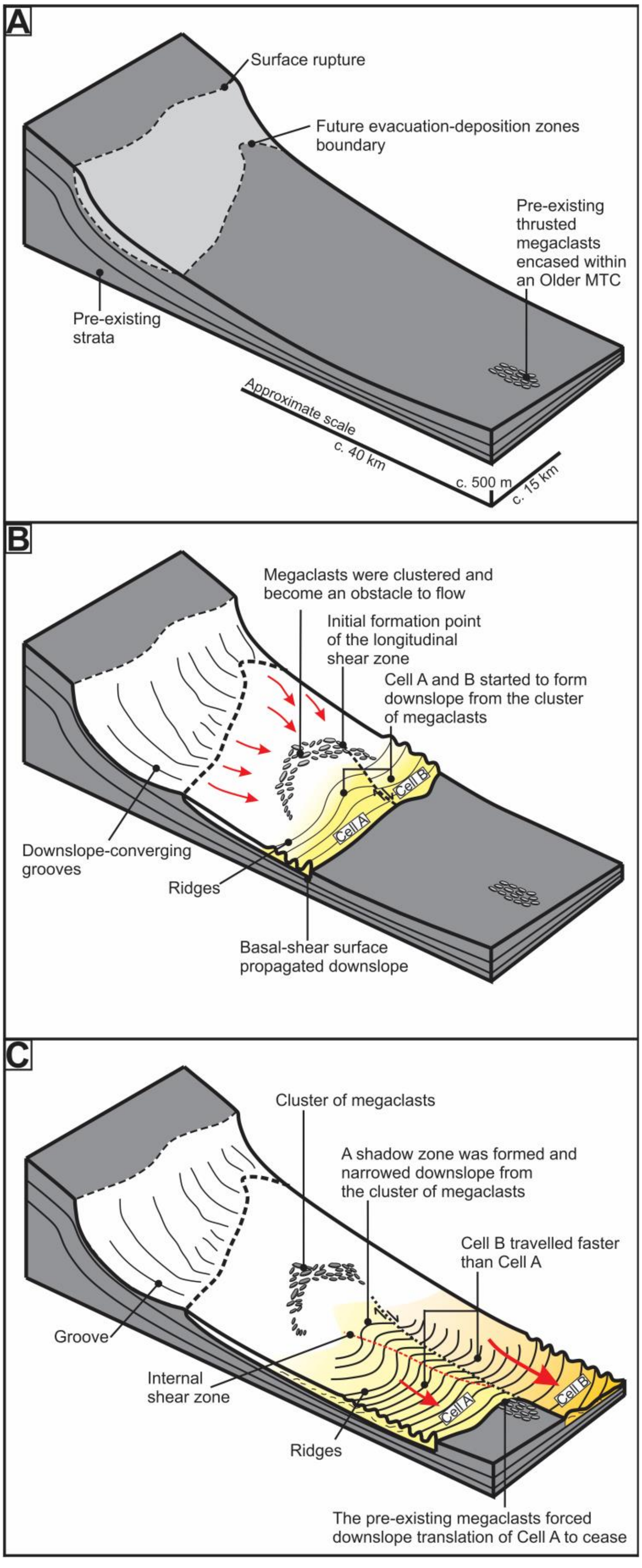

861

862 Figure 13

863